Pervasive nuclear envelope ruptures precede ECM signaling and disease onset without activating cGAS-STING in Lamin-cardiomyopathy mice

Atsuki En[1,2], Hanumakumar Bogireddi[1], Briana Thomas[1], Alexis Stutzman[3], Sachie Ikegami[3], Brigitte LaForest[3], Omar Almakki[3], Peter Pytel[4], Ivan P. Moskowitz[3,4,5], Kohta Ikegami[1,6,7]

[1]Division of Molecular Cardiovascular Biology, Cincinnati Children's Hospital Medical Center, Cincinnati, OH, USA

[2]Graduate School of Nanobioscience, Yokohama City University, Yokohama, Kanagawa, Japan

[3]Department of Pediatrics, The University of Chicago, Chicago, IL, USA

[4]Department of Pathology, The University of Chicago, Chicago, IL, USA

[5]Department of Human Genetics, The University of Chicago, Chicago, IL, USA

[6]Department of Pediatrics, University of Cincinnati College of Medicine, Cincinnati, OH, USA

[7]Corresponding author

SUMMARY

Nuclear envelope (NE) ruptures are emerging observations in Lamin-related dilated cardiomyopathy, an adult-onset disease caused by loss-of-function mutations in Lamin A/C, a nuclear lamina component. Here, we tested a prevailing hypothesis that NE ruptures trigger pathological cGAS-STING cytosolic DNA-sensing pathway, using a mouse model of Lamin-cardiomyopathy. Reduction of Lamin A/C in cardiomyocytes of adult mice caused pervasive NE ruptures in cardiomyocytes, preceding inflammatory transcription, fibrosis, and fatal dilated cardiomyopathy. NE ruptures were followed by DNA damage accumulation without causing immediate cardiomyocyte death. However, cGAS-STING-dependent inflammatory signaling remained inactive. Deleting *cGas* or *Sting* did not rescue cardiomyopathy. The lack of cGAS-STING activation was likely due to the near absence of cGAS expression in adult cardiomyocytes at baseline. Instead, extracellular matrix (ECM) signaling was activated and predicted to initiate pro-inflammatory communication from Lamin-reduced cardiomyocytes to fibroblasts. Our work nominates ECM signaling, not cGAS-STING, as a potential inflammatory contributor in Lamin-cardiomyopathy.

INTRODUCTION

Lamin A/C (*LMNA*) are nuclear lamina proteins that provide structural integrity to the nuclear envelope [1–4]. Mutations in *LMNA* cause a spectrum of degenerative disorders, collectively called laminopathies, including frequent dilated cardiomyopathy (*LMNA*-related DCM) [5–10]. *LMNA*-related DCM is prevalent adult-onset DCM [11,12] that accompanies cardiac conduction disease, fibrosis, heart failure, and mortality [13–16]. *LMNA*-related DCM is predominantly caused by heterozygous loss-of-function *LMNA* mutations that cause Lamin A/C protein reduction most strongly in cardiomyocytes [16–20]. Activation of stress response-related signaling, such as MAPK signaling [21–24], mTOR signaling [25], and DNA damage response signaling [26,27], has been reported in *LMNA*-related DCM models. However, the direct pathological alterations caused by Lamin A/C reduction in cardiomyocytes remain undefined.

Reduction of nuclear lamins can cause ruptures of the nuclear envelope (NE ruptures) [28–31,33–35]. Indeed, NE ruptures have been observed in patients [17,18,32,36,37], animal models [30,31,38–42], and cell culture models [30,35] of *LMNA*-related DCM and laminopathies. However, the extent of NE ruptures in *LMNA*-related DCM and the contribution of this event to the pathogenesis of DCM remain undefined.

A prevailing hypothesis for *LMNA*-related DCM pathogenesis implicates the cGAS-STING pathway as a link between NE rupture, inflammatory signaling, and DCM pathogenesis [39,40,43–45]. cGAS-STING is a cytosolic DNA-sensing innate immune mechanism, in which cGAS binds to cytosolic DNA and activates cell-autonomous STING-mediated interferon transcription [46,47]. cGAS-STING pathway activation has been observed in a cellular model of progeria [48] and *Lmna*-knockout developing hearts [27]. cGAS-STING activation has also been reported in mouse models of other heart diseases [49–52]. However, a direct link between NE ruptures and the cGAS-STING activation in *LMNA*-related DCM remains undefined. In this study, we report pervasive NE ruptures prior to DCM development and provide evidence against the hypothesis that cGAS-STING activation contributes to *LMNA*-related DCM. Instead, our study nominates a role for extracellular matrix signaling from cardiomyocytes in this disease.

60 **RESULTS**

61 **Lamin A/C reduction in cardiomyocytes causes dilated cardiomyopathy in adult mice**

62 We generated a mouse model of *LMNA*-related DCM using cardiomyocyte-specific deletion of *Lmna*
63 (*Lmna*$^{F/F}$*;Myh6-MerCreMer*; *Lmna*^{CKO} hereafter) and littermate control wild-type mice (*Lmna*$^{+/+}$*;Myh6-*
64 *MerCreMer*) (**Fig. S1A, B**). *Lmna* deletion in cardiomyocytes was induced by tamoxifen administration to
65 adult mice at 6-8 weeks of age (**Fig. 1A**). Lamin A and Lamin C proteins were 47% and 43% reduced,
66 respectively, in cardiomyocytes of *Lmna*^{CKO} mice at 2 weeks post tamoxifen, consistent with the 4-week
67 half-life of Lamin A/C in mouse hearts [53] (**Fig. 1B; Fig. S1C**). The reduced, but persistent, Lamin A/C in
68 individual cardiomyocytes was confirmed at 1, 2, and 3.5 weeks post tamoxifen (**Fig. 1C**). Thus, *Lmna*^{CKO}
69 mice reproduced Lamin A/C protein insufficiency, not elimination, observed in cardiomyocytes of *LMNA*-
70 related DCM patients [18,20].

71 *Lmna*^{CKO} mice developed progressive DCM as reported previously (**Fig. 1D, E; Fig. S1D**)[38].
72 Hearts of *Lmna*^{CKO} mice were indistinguishable from wild-type hearts in gross morphology and contractile
73 activity until 2 weeks post tamoxifen. However, at 3 weeks post tamoxifen, left ventricular ejection fraction,
74 an indicator of cardiac systolic function, significantly diminished (**Fig. 1E**). At 3.5 weeks post tamoxifen,
75 *Lmna*^{CKO} hearts became severely dilated, with a significant reduction of ventricular wall thickness and
76 loss of systolic activity. *Lmna*^{CKO} mice invariably died between 3.5 weeks and 4.5 weeks post tamoxifen
77 (**Fig. 1F**). Thus, the modest reduction of Lamin A/C in cardiomyocytes was sufficient to cause DCM that
78 progressed to heart failure, recapitulating a crucial aspect of human *LMNA*-related DCM.

79

80 **Lamin A/C reduction in cardiomyocytes activates inflammation-related transcription**

81 To identify the onset of molecular changes preceding the functional decline of *Lmna*^{CKO} hearts, we profiled
82 the transcriptome of the heart at Days 7, 11, and 14 post tamoxifen by RNA-seq (**Table S1**). At Days 7
83 and 11, the transcriptome of *Lmna*^{CKO} hearts was almost identical to that of wild-type hearts (**Fig. 1G**).
84 However, at Day 14, *Lmna*^{CKO} hearts exhibited strong transcriptional upregulation (1,751 genes) and
85 modest downregulation (351 genes). The upregulated genes were highly overrepresented for gene
86 ontology (GO) terms related to inflammatory responses (**Fig. 1H**). These upregulated genes included
87 innate immune-related genes such as *Cxcl10*, *Ifit1*, and *Irf7* (**Fig. 1I**), which can be activated by the cGAS-
88 STING pathway. The downregulated genes were overrepresented for gene pathways for cardiomyocyte
89 metabolism and function (**Fig. 1H**).

90 We examined whether the upregulation of inflammation-related genes reflected an inflammatory
91 response in *Lmna*^{CKO} hearts. We observed that the CD45+CD68+ macrophage population increased in
92 *Lmna*^{CKO} hearts at 2 weeks post tamoxifen (**Fig. 1J; Fig. S1E**). We also observed increased interstitial
93 collagen deposition at 2 weeks post tamoxifen, which developed into extensive fibrosis by 3.5 weeks post
94 tamoxifen (**Fig. 1K**). Thus, Lamin A/C reduction in cardiomyocytes resulted in extensive upregulation of

95 inflammation-related genes, macrophage expansion, and initial fibrotic response at 2 weeks post
96 tamoxifen, preceding the morphological and functional changes reflective of clinical DCM (**Fig. 1L**).
97
98 ***Lmna^{CKO}* cardiomyocytes develop pervasive localized nuclear envelope ruptures**
99 We examined whether Lamin A/C reduction caused nuclear envelope (NE) ruptures in cardiomyocytes.
100 Strikingly, we observed protrusion of DNA from one or multiple nuclei inside cardiomyocytes in *Lmna^{CKO}*
101 heart sections at 2 weeks post tamoxifen, while this event was absent in wild-type hearts (**Fig. 2A**; of
102 note, 90% of cardiomyocytes are binucleated in adult mice [54]). Nuclei with protruded DNA were positive
103 for Lamin A/C staining, indicating that partial reduction of Lamin A/C was sufficient to cause DNA
104 protrusion (**Fig. 2A**). Electron microscopy revealed strong condensation of protruded DNA that appeared
105 devoid of the surrounding nuclear membrane, suggesting NE ruptures (**Fig. 2B; Fig. S2A**). We isolated
106 cardiomyocytes from hearts at 2 weeks post tamoxifen, immediately fixed them, and examined the
107 nuclear envelope. Lamin A/C signals were specifically lost at the tips of nuclei from which DNA protruded
108 in *Lmna^{CKO}* cardiomyocytes (**Fig. 2C**). The Lamin A/C-lost locations also lost staining for PCM1, a
109 perinuclear matrix protein localized at the cytoplasmic side of the outer nuclear membrane [55] (**Fig. 2D**).
110 The loss of Lamin A/C and PCM1 occurred specifically at the tips of the elongated nuclei positioned along
111 the longitudinal axis of the cardiomyocytes (**Fig. 2A–D; Fig. S2A**). The specific loss of nuclear envelope
112 proteins Lamin A/C and PCM1 at nuclear tips suggested localized NE ruptures in *Lmna^{CKO}*
113 cardiomyocytes.
114 To determine whether NE ruptures occurred in *Lmna^{CKO}* cardiomyocytes, we examined the
115 retention of nuclear-localized tdTomato. We expressed nuclear localization signal (NLS)-fused tdTomato
116 in cardiomyocytes from a transgene *in vivo* and investigated tdTomato localization immediately after
117 cardiomyocyte isolation at 2 weeks post tamoxifen. NLS-tdTomato was localized exclusively to the
118 nucleus in wild-type cardiomyocytes as well as to the intact nuclei in *Lmna^{CKO}* cardiomyocytes (**Fig. 2E;**
119 **Fig. S2B**). However, NLS-tdTomato signals significantly diminished in nuclei with local PCM1 loss in
120 *Lmna^{CKO}* cardiomyocytes (**Fig. 2E, F**). Reciprocally, NLS-tdTomato signals increased in the cytoplasm of
121 *Lmna^{CKO}* cardiomyocytes with PCM1-lost nuclei. NLS-tdTomato leakage from damaged nuclei indicated
122 that the nuclear envelope had ruptured in *Lmna^{CKO}* cardiomyocytes.
123 To quantify NE rupture events, we expressed GFP-tagged catalytically-inactive cGAS (icGAS) in
124 cardiomyocytes *in vivo* using muscle-tropic adeno-associated virus (MyoAAV) [56] (**Fig. 2G**). icGAS is
125 widely used as a "NE rupture marker" owing to the cGAS's affinity to cytoplasmic DNA [57,58]. We observed
126 strong icGAS punctum at every PCM1-lost site on the nuclear envelope in *Lmna^{CKO}* cardiomyocytes at 2
127 weeks post tamoxifen (**Fig. 2H; Fig. S2C**). We found that 66% of *Lmna^{CKO}* cardiomyocytes have at least
128 one nucleus with icGAS puncta on nuclear envelopes, while icGAS puncta were virtually absent in wild-
129 type cardiomyocytes (**Fig. 2I**). Thus, NE ruptures were pervasive in *Lmna^{CKO}* cardiomyocytes at 2 weeks
130 post tamoxifen.

131 To determine whether NE ruptures preceded the transcriptional change, we quantified NE
132 ruptures at Day 11 post tamoxifen, when no transcriptional change was detected (**Fig. 1G**). We used a
133 local loss of PCM1 with concomitant cytoplasmic DNA protrusion as a proxy for NE ruptures, as this
134 feature strongly correlated with icGAS localization. We observed that 31% of *Lmna*^{CKO} cardiomyocytes
135 had at least one ruptured nucleus at Day 11 (**Fig. 2J; Fig. S2D, E**). At Day 14, the NE rupture frequency
136 was 54% based on this method, which was comparable to 66% based on the sensitive icGAS-based
137 quantification (**Fig. 2J**). Thus, about one third of *Lmna*^{CKO} cardiomyocytes developed NE ruptures as
138 early as Day 11 post tamoxifen, preceding the earliest transcriptional changes, with more than 50% of
139 nuclei presenting ruptures by Day 14.
140 We investigated whether the pervasive NE ruptures in *Lmna*^{CKO} cardiomyocytes accompanied
141 DNA damage accumulation (**Fig. 2K; Fig. S2F**). We did not find a statistically significant increase of
142 gamma-H2AX-positive nuclei indicative of DNA double-strand break in *Lmna*^{CKO} hearts at 2 weeks post
143 tamoxifen. In addition, there was no indication of increased cell death assessed by TUNEL at this time
144 point (**Fig. 2L; Fig. S2G**). However, at 3.5 weeks post tamoxifen, gamma-H2AX-positive nuclei
145 significantly increased. Thus, pervasive NE ruptures did not cause immediate DNA damage accumulation
146 or cell death at the time of strong inflammation-related transcriptional upregulation. Instead, DNA damage
147 accumulated when the heart structure and function began to deteriorate (**Fig. 2M**).
148
149 ***Lmna*^{CKO} cardiomyocytes do not activate cGAS-STING-related transcription**
150 Given the pervasive NE ruptures, we tested whether the cGAS-STING cytosolic DNA sensing pathway
151 was activated within *Lmna*^{CKO} cardiomyocytes. In the cGAS-STING pathway, cGAS detection of
152 cytoplasmic DNA activates STING-mediated interferon transcription within cells bearing the cytoplasmic
153 DNA [46,47]. This pathway has been implicated in Lamin A/C-based cardiomyopathy in a previous study [27].
154 cGAS and STING proteins were expressed in the heart, but interestingly, their expression within
155 cardiomyocytes was very low in both wild-type and *Lmna*^{CKO} backgrounds (**Fig. 3A; Fig. S3A, B**). To test
156 whether cGAS-STING-downstream genes were upregulated within cardiomyocytes of *Lmna*^{CKO} hearts,
157 we distinguished cardiomyocyte and non-cardiomyocyte transcriptomes in the heart using SLAM-IT-seq
158 [59]. SLAM-IT-seq labels transcripts in *Cre*-positive cardiomyocytes with 4-thiouracil (4sU) and
159 distinguishes them from unlabeled transcripts from non-cardiomyocyte cells (**Fig. S3C**). As expected,
160 cardiomyocyte-specific genes were specifically 4sU-labeled in wild-type hearts (**Fig. S3D**). We then
161 assessed the labeling state of the 1,020 upregulated genes in *Lmna*^{CKO} hearts and found that 135 genes
162 were 4sU-labeled (i.e. cardiomyocyte-derived) and 885 genes were not 4sU-labeled (i.e. non-
163 cardiomyocyte-derived) in *Lmna*^{CKO} hearts at 2 weeks post tamoxifen (**Fig. 3B**). The cardiomyocyte-
164 originated upregulated genes were not overrepresented for inflammation-related GO terms (**Fig. 3B**) and
165 did not include well-established cGAS-STING downstream genes (**Fig. S3E**; **Table S2**). Instead, these
166 genes were overrepresented for the ECM-related GO terms such as “Proteoglycans in cancer”. On the

167 other hand, non-cardiomyocyte-originated upregulated transcripts were strongly enriched for
168 inflammation-related GO terms (**Fig. 3B**). These data suggested that the cGAS-STING pathway was not
169 activated within *Lmna*^{CKO} cardiomyocytes and that the inflammation-related transcriptional activation
170 originated from non-cardiomyocytes in *Lmna*^{CKO} hearts.

171 We hypothesized that the near absence of cGAS expression prevented cGAS-STING activation
172 within *Lmna*^{CKO} cardiomyocytes. We tested this hypothesis by overexpressing wild-type cGAS in
173 cardiomyocytes *in vivo* with MyoAAV (**Fig. 3C**). We first confirmed that endogenous cGAS was not
174 detectable at NE rupture sites (**Fig. 3D**) and that the well-established cGAS-STING downstream genes,
175 *Cxcl10*, *Ifit3*, and *Ifnb1* [60–63], remained transcriptionally silent in cardiomyocytes of *Lmna*^{CKO} mice
176 transduced with control luciferase MyoAAV (**Fig. 3E**). However, cGAS overexpression in *Lmna*^{CKO}
177 cardiomyocytes resulted in strong cGAS accumulation at NE rupture sites (**Fig. 3D**). Consistently, *Cxcl10*,
178 *Ifit3*, and *Ifnb1* transcripts were 10-, 128-, and 6-fold upregulated, respectively, upon cGAS
179 overexpression (**Fig. 3E**). In wild-type mice, cGAS overexpression did not upregulate cGAS-downstream
180 genes, confirming the NE rupture-dependency of cGAS-downstream activation upon cGAS
181 overexpression. Taken together, these data suggested that *Lmna*^{CKO} cardiomyocytes did not activate the
182 cGAS-STING pathway despite pervasive NE ruptures and that the lack of cGAS-STING activation was
183 likely due to the low cGAS expression in adult cardiomyocytes.
184

185 ***Cgas* and *Sting* are not required for inflammation-related gene expression and DCM in *Lmna*^{CKO}**
186 **mice**

187 We examined the genetic requirement for *Cgas* and *Sting*, the essential mediators of the cGAS-STING
188 pathway, to the inflammation-related transcriptional activation and DCM in *Lmna*^{CKO} hearts. We
189 introduced the germ-line *Cgas*$^{-/-}$ allele [64] into *Lmna*^{CKO} mice or control *Lmna*^{Het} mice
190 (*Lmna*$^{F/+}$*;Myh6MerCreMer*) and validated the absence of cGAS protein in the heart of *Cgas*$^{-/-}$ carriers
191 (**Fig. S3A**). We then performed RNA-seq in whole hearts at 2 weeks post tamoxifen. We first confirmed
192 the expected strong upregulation of inflammation-related genes in *Cgas*$^{+/+}$;*Lmna*^{CKO} hearts compared
193 with *Cgas*$^{+/+}$;*Lmna*^{Het} hearts (**Fig. 3F; Fig. S3F; Table S1**). We then compared *Cgas*$^{-/-}$;*Lmna*^{CKO} hearts
194 with *Cgas*$^{+/+}$;*Lmna*^{CKO} hearts. There was almost no difference in gene expression between them (**Fig.**
195 **3F**). Representative cGAS-STING-downstream genes did not show statistically significant differences in
196 gene expression between *Cgas*$^{-/-}$;*Lmna*^{CKO} and *Cgas*$^{+/+}$;*Lmna*^{CKO} hearts (**Fig. 3G; Fig. S3G**). These data
197 suggested that the inflammation-related transcription in *Lmna*^{CKO} hearts was independent of cGAS.

198 We next combined germ-line *Sting*$^{-/-}$ mice [65] with *Lmna*^{CKO} mice (**Fig. S3B**) and investigated the
199 heart phenotype. By 3.5 to 4 weeks post tamoxifen, *Sting*$^{-/-}$;*Lmna*^{CKO} mice showed as severely reduced
200 left ventricular ejection fraction (**Fig. 3H**) and extensive fibrosis (**Fig. 3I**) as the littermate control
201 *Sting*$^{+/+}$;*Lmna*^{CKO} mice did, whereas *Sting*$^{+/+}$;*Lmna*^{Het} and *Sting*$^{-/-}$;*Lmna*^{Het} mice maintained normal hearts.
202 Likewise, *Cgas*$^{-/-}$;*Lmna*^{CKO} hearts developed severe fibrosis (**Fig. S3H**). Moreover, both *Sting*$^{-/-}$;*Lmna*^{CKO}

203 mice and *Cgas*$^{-/-}$;*Lmna*^{CKO} mice died as early as *Sting*$^{+/+}$;*Lmna*^{CKO} or *Cgas*$^{+/+}$;*Lmna*^{CKO} mice did, whereas
204 no lethality was observed in *Sting*$^{-/-}$;*Lmna*^{Het} and *Cgas*$^{-/-}$;*Lmna*^{Het} mice (**Fig. 3J; Fig. S3I**). Taken
205 together, our data suggested that the cGAS-STING pathway did not mediate inflammatory transcription
206 and the pathophysiologic features of DCM in *Lmna*^{CKO} hearts (**Fig. 3K**).
207
208 **Cardiomyocytes, fibroblasts, and immune cells are transcriptionally altered in *Lmna*^{CKO} hearts**
209 We explored alternative mechanisms by which Lamin A/C reduction in cardiomyocytes caused DCM. To
210 identify intercellular signaling initiated by *Lmna*^{CKO} cardiomyocytes, we defined the cell type-resolved
211 transcriptional changes using single-nucleus (sn) RNA-seq (**Table S3**). We obtained transcriptomes for
212 14,111 nuclei from either wild-type or *Lmna*^{CKO} hearts at 2 weeks post tamoxifen (n=3; **Fig. 4A**). These
213 nuclei were grouped into cardiomyocytes (CM1 and CM2), fibroblasts (Fib1 and Fib2), macrophages
214 (Mac1 and Mac2), T cells, endothelial cells (coronary, lymphatic, and other), pericytes, or neurons, based
215 on their transcriptomes (**Fig. S4A**). Among these, CM2, Fib2, Mac2, and T-cells were highly
216 overrepresented by *Lmna*^{CKO} heart-derived cells (**Fig. 4B; Fig. S4B**). CM2 was characterized by high
217 *Rtn4* expression, a feature also reported in *Lmna*-knockout myotubes [66] and Lamin A/C-independent
218 heart disease [67–70] (**Fig. S4A**). Fib2 was characterized by myofibroblast marker *Postn* [71], Mac2 by
219 circulating monocytic receptor *Ccr2* [72], and T cells by T cell adaptor *Skap1* [73]. We found extensive
220 differential gene expression within cardiomyocytes (CM1 and CM2 combined), fibroblasts (Fib1 and Fib2
221 combined), and immune cells (Mac1, Mac2, T cell combined) while other cell types exhibited almost no
222 expression differences (**Fig. 4C, D; Fig. S4C; Table S4**). The upregulated genes in cardiomyocytes were
223 not overrepresented for cytosolic DNA sensing pathway, did not include cell death-related genes, but
224 included some DNA damage repair-related genes, as expected (**Fig. S4D–F**).
225 Interestingly, upregulated genes in *Lmna*^{CKO} cardiomyocytes and those in fibroblasts were both
226 most strongly overrepresented for ECM-related pathways (**Fig. 4D**). The upregulated ECM-related genes
227 included collagen and integrin genes (in cardiomyocytes and fibroblasts) and ECM proteinase and
228 crosslinker genes (specifically in fibroblasts) (**Fig. 4E**). On the other hand, fibroblasts and immune cells,
229 but not cardiomyocytes, commonly upregulated immune-related genes including cytokine, cytokine
230 receptor, and cytokine transcription factor genes (**Fig. 4D, F**). These results suggested potential signal
231 crosstalk between cardiomyocytes and fibroblasts and between fibroblasts and immune cells in *Lmna*^{CKO}
232 hearts.
233
234 **ECM-mediated signaling from *Lmna*^{CKO} cardiomyocytes is predicted to activate fibroblasts**
235 We investigated intercellular signal crosstalk in *Lmna*^{CKO} hearts by applying the CellChat program [74] to
236 the snRNA-seq data. This analysis predicted ECM-receptor signaling from CM2 to Fib2 as the only
237 strongly upregulated signaling originating from CM2, the population predominantly consisted of *Lmna*^{CKO}
238 cardiomyocyte nuclei (**Fig. 4G, Box a**). Collagens and laminins were predicted to mediate this CM2-to-

239 Fib2 signaling (**Fig. 4H**). CM2 were not predicted to signal directly to immune cell populations. Instead,
240 Fib2 were predicted to send ECM-mediated signals to CM2 (**Box b**), Fib2 (**Box c**), and T cells (**Box d**),
241 via collagens, laminins, thrombospondins, and fibronectins (**Fig. 4G, H**). Fib2 were also predicted to send
242 secretion-mediated signals to Fib2 (**Box e**), and Mac2 (**Box f**), via ANGPTL (angiopoietin-like), TGF beta,
243 BMP, and SEMA3 (semaphorin3). Fib2 might therefore act as a central signaling hub, receiving signals
244 from CM2 and sending signals to immune cells (**Fig. 4I**). Finally, Mac2 were predicted to send secretion-
245 mediated signals to Mac2 themselves (**Box g**) via CCL (chemokine ligands), SPP1 (osteopontins), and
246 complement factors. This signaling might mediate the macrophage infiltration observed in *Lmna*^{CKO}
247 hearts (**Fig. 1J**). Taken together, our results suggested that *Lmna*^{CKO} cardiomyocytes activated
248 fibroblasts via ECM-mediated signaling, not cytokine-mediated signaling such as cGAS-STING, and that
249 fibroblasts activated and recruited immune cells through both ECM signaling and secretion signaling to
250 orchestrate inflammatory signaling in the heart (**Fig. 4J**).
251

252 **DISCUSSION**

253 We report that frequent localized NE ruptures precede transcriptional changes, DNA damage
254 accumulation, and heart functional decline in *Lmna*^{CKO} hearts. Given our observation that a 50% reduction
255 of Lamin A/C proteins is sufficient to induce pervasive NE ruptures in cardiomyocytes, NE ruptures might
256 be more prevalent than previously anticipated in *LMNA*-related DCM. NE ruptures might have been
257 overlooked due to the specific location of localized NE ruptures at the tips of elongated nuclei within
258 cardiomyocytes. The mechanisms underlying NE ruptures and the causal role of NE ruptures in DCM
259 remain to be investigated.

260 Our data indicate that the cGAS-STING pathway does not contribute to *LMNA*-related DCM in
261 the adult mouse model investigated herein. This suggests that pharmacologically reducing cGAS-STING
262 activity for treating *LMNA*-related DCM, an idea previously discussed [27,75], may be ineffective. Our
263 conclusion diverges from a previous report that *Cgas* deletion can delay early postnatal cardiomyopathy
264 caused by *Lmna* deletion in embryonic hearts [27]. This difference may be due to that the near absence of
265 cGAS expression prevents cGAS-STING activation in adult cardiomyocytes, whereas the basal cGAS-
266 STING activity may be higher in early postnatal cardiomyocytes [76,77]. The lack of robust cGAS expression
267 may reduce pathogen-derived DNA sensing in adult cardiomyocytes, similar to hepatocytes that also lack
268 functional cGAS-STING [78]. Many reports suggest an association between DNA damage and cGAS-
269 STING activation [27,79–82]. Our data that *Lmna*^{CKO} cardiomyocytes accumulate DNA damage without
270 activating cGAS-STING suggest that DNA damage and cGAS-STING can be uncoupled.

271 Our study nominates ECM signaling as a mechanism by which Lamin A/C-reduced
272 cardiomyocytes initiate an inflammatory response by activating fibroblasts. A recent study reported a
273 similar observation in which NE rupture induces ECM remodeling through unknown mechanisms that
274 require DNA damage [83]. Further study on the potential roles of ECM signaling in *LMNA*-related DCM is
275 required.

276

277 ***Limitations of the study***

278 We reduced Lamin A/C exclusively within the cardiomyocytes of adult mice. Whether Lamin A/C
279 reduction in other cell types or at other stages causes NE ruptures and contributes to DCM through
280 cGAS-STING activation remains an open question.

281

ACKNOWLEDGEMENT

We thank core facilities for animal care, microscopy, genomics, and pathology at Cincinnati Children's and the University of Chicago for their assistance. This work is supported by NIH grant R21/R33 AG054770 (K.I.), Cincinnati Children's Research Innovation and Pilot grant (K.I.), NIH grants R01 HL163523, R01 HL124836, and R01 HL126509 (I.P.M).

AUTHOR CONTRIBUTION

Conceptualization, A.E. and K.I.; Methodology, A.E., I.P.M., and K.I.; Formal Analysis, A.E. and K.I.; Investigation, A.E., H.B., B.T., A.S., S.I., B.L., O.A., P.P., K.I.; Resources, I.P.M.; Data Curation, A.E. and K.I; Writing – Original Draft, A.E., and K.I.; Writing – Review & Editing, A.E., I.P.M., and K.I.; Visualization, A.E. and K.I.; Supervision, K.I.; Project Administration, K.I.; Funding Acquisition, K.I. and I.P.M.

DECLARATION OF INTERESTS

The authors declare no competing interests.

297 **FIGURE LEGENDS**

298 **Figure 1. Lamin A/C reduction in cardiomyocytes causes dilated cardiomyopathy in adult mice**

299 **A)** Tamoxifen (Tam) induces *Lmna* deletion in cardiomyocytes in adult mice. See **Fig. S1** for related
300 analyses.

301 **B)** Lamin A/C immunoblot in isolated cardiomyocytes (top) with signal quantification (bottom).

302 **C)** Lamin A/C immunohistochemistry (brown) with hematoxylin counterstaining (blue) in mouse heart
303 tissues. Scale bar: 20 μm.

304 **D)** Hematoxylin-eosin staining of hearts. Scale bar: 1 mm.

305 **E)** Left ventricular ejection fraction with interquartile range (box) measured by echocardiography.

306 **F)** Kaplan-Meier survival analysis.

307 **G)** Volcano plot comparing RNA-seq read counts in $Lmna^{CKO}$ versus WT hearts. Up, upregulated gene
308 count. Down, downregulated gene count.

309 **H)** The top 10 Gene Ontology terms overrepresented among differentially expressed genes.

310 **I)** Normalized RNA-seq gene expressed levels for immune-related genes (bar, mean).

311 **J)** Immunofluorescence of heart tissue sections for CD45 (pan-leukocyte, red) and CD68 (macrophage,
312 green). Scale bar: 20 μm.

313 **K)** Masson's trichrome staining of heart sections. Arrow, collagen deposition. Scale bar: 20 μm.

314 **L)** Summary

315

316 **Figure 2. Lamin A/C reduction causes localized nuclear envelope rupture in cardiomyocytes**

317 **A)** Lamin A/C immunohistochemistry in heart tissue. Arrow, DNA protruded from nuclei. Scale bar: 20 μm.
318 See **Fig. S2** for related analyses.

319 **B)** Top: Transmission electron micrograph of heart sections focusing on cardiomyocytes. Bottom: Close-
320 up image of the area indicated by rectangle in upper panel. Arrow, protruded chromatin. Scale bar: 1 μm.

321 **C)** Immunofluorescence for Lamin A/C in isolated cardiomyocytes. Phalloidin stains F-actin. Arrowhead,
322 local loss of Lamin A/C with protruded DNA. Scale bar: 20 μm.

323 **D)** Same as **(C)**, but for PCM1.

324 **E)** NLS-tdTomato signals in isolated cardiomyocytes co-stained for PCM-1. Scale bar: 20 μm.

325 **F)** NLS-tdTomato signal intensity in nucleus and cytoplasm of cardiomyocytes (box, interquartile range).
326 $Lmna^{CKO}$ cardiomyocytes are stratified by the presence or absence of local PCM-1 loss at the nuclear
327 envelope. WT n=51, $Lmna^{CKO}$ n=53 (PCM1-loss 34, intact 19) cardiomyocytes.

328 **G)** MyoAAV-mediated GFP-icGAS expression in cardiomyocytes *in vivo*.

329 **H)** GFP-icGAS signals in isolated cardiomyocytes co-stained for PCM1. Scale bar: 20 μm.

330 **I)** Percentage of cardiomyocytes with GFP-icGAS punctum at nuclear tip (bar, mean).

331 **J)** Percentage of cardiomyocytes with DNA protrusion from PCM1-lost nuclear tip (bar, mean) at 11 days
332 (left) and 14 days (right) post tamoxifen.

333 **K)** Percentage of gamma-H2AX-positive nuclei in heart section (bar, mean).
334 **L)** Number of TUNEL-positive cells in heart section (bar, mean).
335 **M)** Summary
336
337 **Figure 3. *Cgas* and *Sting* are not required for inflammation-related gene expression and dilated**
338 **cardiomyopathy in *Lmna^{CKO}* mice**
339 **A)** Normalized cGAS and STING abundance quantified by immunoblot shown in **Fig. S3A, B** (bar, mean).
340 **B)** Left: Upregulated genes in *Lmna^{CKO}* hearts at 2 weeks post tamoxifen are categorized into
341 cardiomyocyte-derived or non-cardiomyocyte-derived based on 4sU labeling in SLAM-IT-seq. Right: GO
342 terms enriched among each class of upregulated genes.
343 **C)** MyoAAV-mediated GAS overexpression in cardiomyocytes *in vivo*.
344 **D)** Top: Anti-cGAS and Lamin A/C immunofluorescence in isolated cardiomyocytes. Bottom: Close-up
345 image of the area indicated by rectangle in upper panel. Arrowhead, GFP-icGAS localization at nuclear
346 tip. Scale bar: 20 μm.
347 **E)** Transcript abundance in isolated cardiomyocytes quantified by quantitative PCR and normalized by
348 *Actb* transcripts (bar, mean).
349 **F)** Volcano plot comparing RNA-seq read counts in *Cgas$^{-/-}$*; *Lmna^{Het}* (n=4) versus *Cgas$^{+/+}$*; *Lmna^{Het}* (n=6)
350 (left) and in *Cgas$^{-/-}$*; *Lmna^{CKO}* (n=4) versus *Cgas$^{+/+}$*; *Lmna^{CKO}* (n=6) (right).
351 **G)** Normalized RNA-seq gene expressed levels for cGAS-STING-related genes (bar, mean).
352 **H)** Left ventricular ejection fraction measured by echocardiography (box, interquartile range).
353 **I)** Masson's trichrome staining of heart sections. Scale bar: 20 μm.
354 **J)** Kaplan-Meier survival analysis.
355 **K)** Summary
356
357 **Figure 4. ECM-mediated signaling from *Lmna^{CKO}* cardiomyocytes is predicted to activate**
358 **fibroblasts**
359 **A)** snRNA-seq UMAP plot for 14,111 nuclei from either WT or *Lmna^{CKO}* hearts, colored by cell-type
360 annotation. CM, cardiomyocyte. Fib, fibroblast. Mac, macrophage. EC, endothelial cell. CEC, coronary
361 EC. LEC, lymphatic EC. PC, pericyte. See **Fig. S4** for additional analyses.
362 **B)** Count of WT and *Lmna^{CKO}* heart-originating nuclei within each cell type cluster. Cell types combined
363 in later analyses are indicated below graph.
364 **C)** Pseudo-bulk volcano plot comparing sbRNA-seq read counts in cells of *Lmna^{CKO}* hearts versus cells
365 of WT hearts within each cell type. Red, upregulated genes. Blue, downregulated genes.
366 **D)** GO terms enriched among upregulated genes within indicated cell type. Red arrows, ECM-related GO
367 term. Blue arrow, inflammation-related GO term.

368 **E)** Pseudo-bulk transcript abundance of ECM-related genes. Point, mean of normalized read count per
369 replicate. Bar, mean across replicates.
370 **F)** Same as (E), but for immune-related genes.
371 **G)** Predicted signaling strength between sender cells (x-axis) and receiver cells (y-axis). Color indicates
372 the extent of signaling gains in *Lmna*^{CKO} hearts relative to WT hearts.
373 **H)** Predicted signaling mediators for the signaling indicated by box in (**G**) with alphabetical labels.
374 **I)** Predicted intercellular signaling (indicated in **G** by alphabet labels) in *Lmna*^{CKO} hearts.
375 **J)** Model
376
377

SUPPLEMENTARY FIGURE LEGENDS

Figure S1. Characterization of adult mice with cardiomyocyte-specific *Lmna* deletion

A) Immunofluorescence for PCM1, NLS-tdTomato, and COX4 in heart sections. PCM1 and COX4 are used to stain cardiomyocyte nuclei and the cytoplasm, respectively. Scale bar: 20 μm.

B) Left: Schematic for the *Lmna* LoxP allele and the expected recombined allele upon Cre expression. Arrow, PCR primer location. Right: Amplification of the wild-type, floxed, and recombined *Lmna* alleles by PCR using primers indicated in the left panel. The recombination efficiency (%) was calculated by the intensity of the 153-bp recombined band over the intensity of the 598-bp floxed band.

C) The whole immunoblot for **Fig. 1B**, with Coomassie staining of the original gel.

D) Echocardiography of left ventricular (LV) geometry. P, Wilcoxon test.

E) Quantification of CD45 and CD68-positive cells in heart sections. Representative image in **Fig. 1J**.

Figure S2. Characterization of nuclear envelope ruptures in *Lmna*^{CKO} cardiomyocytes

A) Top: Additional transmission electron micrographs of heart sections focusing on cardiomyocytes, related to **Fig. 2B**. Bottom: Enlarged images of the area indicated by yellow box in the upper panels. Arrow, protruded chromatin. Scale bar: 1 μm.

B) Additional immunofluorescence images for PCM-1 with detection of native NLS-tdTomato. Scale bar: 20 μm.

C) Immunofluorescence for PCM-1 with detection of exogenous GFP-icGAS in isolated cardiomyocytes, related to **Fig. 2H**. Phalloidin stains F-actin. Arrowhead, GFP-icGAS localization at nuclear tips. Scale bar: 20 μm.

D) Immunofluorescence images for PCM1 in isolated cardiomyocytes at Day 11 post tamoxifen. Arrowhead, local loss of PCM1 at nuclear tips. Scale bar: 20 μm.

E) Fraction of cardiomyocytes with DNA protrusion from PCM1-lost nuclear tips. Cardiomyocytes are stratified by the number of ruptured nuclei per cell. Only multinucleated cardiomyocytes are analyzed.

F) Immunofluorescence for γH2AX and desmin in heart tissue sections. Desmin stains cardiomyocytes. Arrowhead, γH2AX-stained nuclei. Scale bar: 20 μm.

G) TUNEL assay for cell death detection in heart tissues. Arrowhead, TUNEL-positive cells. Scale bar: 20 μm.

Figure S3. Analysis of the cGAS-STING pathway in *Lmna*^{CKO} hearts

A) cGAS and GAPDH immunoblots, and Coomassie staining of original gel, in hearts and isolated cardiomyocytes, related to **Fig. 3A**.

B) Same as (A), but for STING.

C) Principle of SLAM-IT-seq. Transcripts in cardiomyocytes are labeled by 4-thiouracil (4sU).

413 **D)** SLAM-IT-seq data for all genes in WT hearts at 2 weeks post tamoxifen, with the expression level on
414 the X axis and the 4sU labeling frequency on the Y axis. Select genes known to be preferentially
415 expressed in cardiomyocytes (red) and those not known to be preferentially expressed in cardiomyocytes
416 (black) are indicated.
417 **E)** SLAM-IT-seq data for the 1,020 upregulated genes at 2 weeks post tamoxifen, with the rank order of
418 the fold change of upregulation on the X axis and the 4sU labeling frequency in *Lmna*^{CKO} hearts on the Y
419 axis. All cytokine genes among the upregulated genes, which are all among unlabeled genes (blue), are
420 indicated. Highly labeled genes (Log_{10} P-value > 3.5) are also indicated (orange).
421 **F)** The top 10 Gene Ontology terms overrepresented among differentially expressed genes in *Cgas*$^{-/-}$;
422 *Lmna*^{Het} versus *Cgas*$^{+/+}$; *Lmna*^{Het}.
423 **G)** Normalized RNA-seq gene expressed levels for additional cGAS-STING-related genes (bar, mean).
424 **H)** Masson's trichrome staining of heart sections. Scale bar: 20 μm.
425 **I)** Kaplan-Meier survival analysis.
426
427 **Figure S4. Single-nucleus RNA-seq analysis of *Lmna*^{CKO} hearts**
428 **A)** Expression (sum of single-nucleus normalized read count across 3 mice within cell type) of maker
429 genes used to classify single nuclei to the cell types indicated along the Y axis, related to **Fig. 4A.**
430 **B)** snRNA-seq UMAP plot for 14,111 nuclei, colored by sample genotype. Inset, UMAP colored by cell
431 type for reference.
432 **C)** GO terms enriched among downregulated genes within indicated cell type.
433 **D)** Enrichment for select GO terms relevant to cytosolic DNA sensing among upregulated genes.
434 **E)** Expression (mean of single-nucleus normalized read count within cell type) of cell death-related genes.
435 Dot, mean within individual mice. Bar, mean across three mice.
436 **F)** Same as (C), but for DNA damage repair-related genes.
437
438 **SUPPLEMENTARY TABLES**
439 **Table S1.**
440 Differentially expressed genes identified by bulk RNA-seq, related to **Figures 1 and 3**. The table includes
441 differentially expressed genes between wild-type and *Lmna*^{CKO} hearts at 1 week post tamoxifen, 11 days
442 post tamoxifen, and 2 weeks post tamoxifen, and for *Cgas/Lmna* double-knockout experiment.
443
444 **Table S2.**
445 Normalized expression values, C-to-T conversion rates, and beta-binomial test P-values for SLAM-IT-
446 seq data, related to **Figure 3**.
447

448 **Table S3.**

449 Indexed oligonucleotides used in snRNA-seq, related to **Figure 4**, including indexed RT primers, indexed
450 ligation primers, and indexed P7 PCR primers.

451

452 **Table S4.**

453 Differentially expressed genes between cells of wild-type and *Lmna*^{CKO} hearts, derived from pseudo-bulk
454 analysis of snRNA-seq data, related to **Figure 4**.

455

456

457 **METHODS**

458

459 **Resource availability**

460 **Lead contact**

461 Kohta Ikegami (email: Kohta.Ikegami@cchmc.org).

462

463 **Materials availability**

464 All mice are available at the sources specified in **Key Resources Table**. Plasmids produced in this study
465 are provided upon request from the lead contact after material transfer agreements. Any information
466 required to reanalyze the data reported in this paper is available from the lead contact.

467

468 **Data availability**

469 High-throughput sequencing data associated with this version of the manuscript are limited to reviewers
470 and journal editors. All data will become available to the public after peer review.

471

472 **Method details**

473 **Mouse genetics and treatment**

474 *Lmna-LoxP* mice [84] were provided by Dr. Yixian Zheng at Carnegie Institution. *Myh6-MerCreMer*
475 (Myh6MCM) transgene mice [85] (JAX stock No: 005657), *Rosa26*$^{CAG\text{-}LSL\text{-}tdTomato}$ ("Ai75") mice [86] (JAX stock
476 No: 25106), *Cgas-null* mice [64] (JAX stock No: 026554), and *CAG-Lox-Stop-Lox-Uprt* transgene mice [87]
477 (*Uprt*^{Tg}; JAX stock No: 021469) were obtained from the Jackson Laboratory. *Sting-null* mice were
478 generated by breeding *Sting-flox* mice [65], obtained from the Jackson Laboratory (JAX stock No: 031670),
479 with mice carrying the *Mef2C-AHF-Cre* transgene allele [88], provided by Dr. Brian L. Black at the University
480 of California San Francisco. For cardiomyocyte-specific *Lmna* knockout experiments,
481 *Lmna*$^{F/F}$*;Myh6MCM*$^{Tg/0}$ (*Lmna*^{CKO}) and *Lmna*$^{+/+}$*;Myh6MCM*$^{Tg/0}$ (wild-type control) mice were used. For the
482 analysis of nuclear tdTomato intensity, *Lmna*$^{F/F}$*;Myh6MCM*$^{Tg/0}$;*Rosa26*$^{CAG\text{-}LSL\text{-}tdTomato/+}$ and
483 *Lmna*$^{+/+}$*;Myh6MCM*$^{Tg/0}$;*Rosa26*$^{CAG\text{-}LSL\text{-}tdTomato/+}$ mice were used. For SLAM-IT-seq experiments,
484 *Lmna*$^{F/F}$*;Myh6MCM*$^{Tg/0}$*;Uprt*$^{Tg/0}$, *Lmna*$^{+/+}$*;Myh6MCM*$^{Tg/0}$*;Uprt*$^{Tg/0}$, *Lmna*$^{F/F}$*;Myh6MCM*$^{Tg/0}$*;Uprt*$^{0/0}$, and
485 *Lmna*$^{+/+}$*;Myh6MCM*$^{Tg/0}$*;Uprt*$^{0/0}$ mice were used. For *Cgas* deletion experiments, *Cgas*$^{-/-}$*;Lmna*$^{F/F}$*;Myh6MCM*$^{Tg/0}$
486 mice, *Cgas*$^{+/+}$;*Lmna*$^{F/F}$*;Myh6MCM*$^{Tg/0}$, *Cgas*$^{+/+}$;*Lmna*$^{F/+}$*;Myh6MCM*$^{Tg/0}$, and *Cgas*$^{-/-}$*;Lmna*$^{F/+}$*;Myh6MCM*$^{Tg/0}$
487 mice were used. For *Sting* deletion experiments, *Sting*$^{-/-}$;*Lmna*$^{F/F}$*;Myh6MCM*$^{Tg/Tg}$
488 mice, *Sting*$^{+/+}$;*Lmna*$^{F/F}$*;Myh6MCM*$^{Tg/Tg}$, *Sting*$^{+/+}$;*Lmna*$^{F/+}$*;Myh6MCM*$^{Tg/Tg}$, and *Sting*$^{-/-}$;
489 *Lmna*$^{F/+}$*;Myh6MCM*$^{Tg/Tg}$ mice were used. All mice used in experiments were administered with tamoxifen
490 (Sigma, T5648) at 6-8 weeks of age via intraperitoneal injections (100 μL of 4 mg/mL solution per day for
491 4 consecutive days) dissolved in corn oil (Sigma, C8267). All mice were used in mixed genetic
492 backgrounds. All mouse experiments were approved by the Institutional Animal Care and Use Committee

493 (IACUC) at Cincinnati Children's Hospital under IACUC protocol 2021-0014 or at University of Chicago
494 under IACUC protocol 71730-10. All procedures were performed in compliance with institutional and
495 governmental regulations under PHS Animal Welfare Assurance number D16-00068 (Cincinnati
496 Children's) or D16-00322 (University of Chicago).
497
498 **Mouse genotyping**
499 For genotyping of the *Lmna* alleles, genomic DNA of isolated cardiomyocytes was extracted with
500 Phenol/Chloroform/Isoamyl alcohol (Invitrogen,15593-031), treated with RNaseA and Proteinase K, and
501 purified. Floxed, recombined, and wild type *Lmna* alleles were detected by PCR using the primers KI279
502 and KI280 (**Key Resources Table**). Based on the agarose gel (1.5%) analysis of PCR-amplified
503 products, recombination efficiency (%) was calculated by 153-bp band (Recombined) over 598-bp band
504 (Floxed) intensities. Genotyping of *Myh6-MerCreMer*, *Cgas*, *Sting*, *Uprt*, and *Rosa26::CAG-LSL-*
505 *tdTomato* alleles was performed at Transnetyx, Inc.
506
507 **Echocardiography**
508 The transthoracic echocardiography was performed using a Vevo 3100 LT (FUJI FILM VisualSonics) and
509 a transducer of 50-MHz MX-700. Parasternal long-axis view and short-axis view at the papillary muscle
510 level were imaged. Two-dimensional M-mode tracing was recorded at three or more consecutive cardiac
511 cycles. Data were analyzed using Vevo LAB Software Package V3.2.6. Echocardiographic parameters
512 between two groups were compared using Wilcoxon rank sum tests, and P-values were adjusted for
513 multiple testing using the Benjamini-Hochberg procedure in R.
514
515 **Survival analysis**
516 Kaplan-Meier survival analyses were performed using the *survival* package and visualized using the
517 *survminer* package in R. Log-rank tests were performed using the *survdiff* function in the survival
518 package.
519
520 **Histological staining**
521 Hearts were perfused with 100 mM KCl and fixed in 10% Formalin (Fisherbrand, 245-685). Fixed hearts
522 were embedded in paraffin and sectioned to a thickness of 5 μm. Heart sections were stained with
523 hematoxylin and eosin (H&E) or a Masson's Trichrome Kit (Thomas Scientific LLC, KTMTRPT) according
524 to the manufacturer's protocol.
525
526 **Cardiomyocyte isolation**
527 Mice were administered with heparin (100 Units, NDC 25021-400-10), anesthetized with Isoflurane, and
528 euthanized by cervical dislocation. Hearts were perfused with 100 mM KCl and moved to Tyrode's

529 solution (10 mM glucose, 5 mM HEPES, 5.4 mM KCl, 1.2 mM $MgCl_2$, 150 mM NaCl and 2 mM sodium
530 pyruvate, pH 7.35). Excised hearts were cannulated to the Langendorff retrograde perfusion system
531 through the aorta and perfused with Base solution (Tyrode's solution with 10 mM taurine and 12 mM
532 2,3-butanedione monoxime) and then digested with prewarmed Digestion buffer (Base solution with 180
533 U/mL Collagenase Type II (Worthington, LS004177) and 25 μM $CaCl_2$) for 20 minutes at 37°C. Heart
534 tissue was then isolated, gently minced in Base solution containing 5 mg/mL BSA. Cell suspension was
535 filtrated through a 240 μm mesh. Cardiomyocytes settled to the bottom of conical tubes by gravity were
536 used in experiments.
537
538 **Immunohistochemistry**
539 Deparaffinized heart tissue sections, that had been fixed with 10% formalin, were subjected to heat-
540 induced antigen retrieval in Target Retrieval Solution (S2367, DAKO) for 5 minutes. Antigen-retrieved
541 sections were incubated with anti-Lamin A/C antibody Ab26300 (rabbit, Abcam) (1:400) for 1 hour at
542 room temperature, followed by biotinylated anti-rabbit IgG antibody for 30 minutes at room temperature.
543 The antigen-antibody binding was detected by Elite kit (PK-6100, Vector Laboratories) and DAB (DAKO,
544 K3468) system. Sections were counterstained by hematoxylin.
545
546 **Immunofluorescence on tissue sections**
547 Deparaffinized heart tissue sections, that had been fixed with 10% formalin, were subjected to heat-
548 induced antigen retrieval in 10 mM Tris EDTA buffer (pH 9.0) for 5 minutes. Antigen-retrieved sections
549 were incubated overnight at 4 °C with goat anti-CD45 antibody (R&D Systems, AF114-SP) and rabbit
550 anti-CD68 antibody (Cell Signaling, 97778), or rabbit anti-γ-H2A.X antibody (Cell Signaling, 9718) and
551 goat anti-desmin antibody (Invitrogen, PA5-19063), or rabbit anti-PCM1 antibody (Sigma, HPA023370),
552 goat anti-TdTomato antibody (OriGene, AB8181), and mouse anti-Cox4 antibody (R&D Systems,
553 MAB6980), followed by Alexa fluorophore-conjugated secondary antibodies for 1 hour at 37°C. Cells
554 were counterstained with DAPI (4′,6-diamidino-2-phenylindole), submerged in 0.25% Sudan Black B
555 (Electron Microscopy Slides, #21610) in 70% Isopropanol for 10 minutes, and then mounted with ProLong
556 Glass Antifade Mountant (Invitrogen, P36984). Fluorescence signals and imaging were acquired using a
557 Nikon A1R laser-scanning confocal microscope. CD45 and CD68 quantification of whole heart tissue was
558 performed using Nikon NIS-Elements; each genotype had five biological replicates. CD45/CD68 positive
559 cells were identified based on the overlap of the DAPI signal with CD45/CD68. Signal intensities between
560 two groups were compared using Wilcoxon rank sum tests in R. For γ-H2A.X quantification, nuclei with
561 DAPI were counted and those with at least one γ-H2A.X focus were quantified using CellProfiler. Five to
562 eight images per mouse (374 x 374 μm^2 per image) were used for the quantification.
563

564 **Immunofluorescence on isolated cardiomyocytes**

565 Isolated cardiomyocytes were fixed in 4% paraformaldehyde (Electron Microscopy Slides, #15710) in
566 PHEM buffer (60 mM PIPES pH7.5, 25 mM HEPES pH7.5, 10 mM EGTA, 4 mM $MgSO_4$) for 10 minutes
567 at 37°C, then washed with PBS and attached to coverslips with Cell-Tak Cell Adhesive (Sigma Aldrich,
568 354240). Cells were blocked and permeabilized with in a buffer containing 5% normal donkey serum
569 (Jackson ImmunoResearch, 017-000-121), 1% non-fat milk, and 0.1% Triton X-100 in PBS for 1 hour at
570 37°C. Permeabilized cells were incubated overnight at 4°C with mouse anti-Lamin A/C antibody (Santa
571 Cruz, sc-376248), rabbit anti-PCM-1 antibody (Sigma, HPA023370), mouse anti-cGAS antibody (Cell
572 Signaling, D3O8O). Cells were washed and incubated with Alexa fluorophore-conjugated secondary
573 antibodies and Alexa Fluor Plus 647 Phalloidin for 1 hour at 37°C. Cells were counterstained with DAPI
574 and then mounted with ProLong Glass Antifade Mountant. Fluorescence signals were detected on Nikon
575 A1R laser-scanning confocal microscope or Yokogawa CSU-W1 Sora spinning disk confocal microscope.
576

577 **Plasmid construction**

578 The expression vectors used in this study were derived from the pAAV:cTNT::Luciferase vector (gift from
579 William Pu; Addgene plasmid # 69915) [89]. For cloning of pAAV:cTnT::cGAS and pAAV:cTnT::GFP
580 vectors, we digested the pAAV:cTNT::Luciferase vector with *NheI* and *NotI*, and the luciferase gene was
581 replaced with the cGAS or EGFP sequences using NEBuilder HiFi DNA Assembly Master Mix (NEB
582 E2621). The pAAV:cTnT::GFP-icGAS vector was generated by inserting the catalytically-inactive cGAS
583 (icGAS) sequence (DNA fragment ID: EA086, **Key Resources Table**) into the pAAV:cTnT::GFP vector
584 digested with *NotI*. The icGAS sequence was derived from the human cGAS protein sequence with an
585 E225A/D227A amino acid substitution that abolishes enzyme activity and interferon production, but
586 retains DNA binding ability and functions, used as a NE rupture marker previously [57]. The DNA fragments
587 for mouse wild-type *Cgas* (NM_173386.5) and *icGAS* were synthesized using gBlocks Gene Fragment
588 synthesis service (Integrated DNA Technologies). *EGFP* with a flexible GS linker (GGGGS) at the C-
589 terminus [90] was amplified from the pLJM1-EGFP vector (gift from David Sabatini; Addgene plasmid
590 #19319) [91] using the EA062 and EA064 primers (**Key Resources Table**).
591

592 **MyoAAV production and *in vivo* transduction**

593 For myoAAV production, we used a published protocol with modifications [92]. We co-transfected the
594 pAAV-cTnT-transgene vector (see above), the pHelper vector (GenBank: AF369965.1), and the
595 pRep/Cap 1A-MYO capsid vector [56] into AAVpro 293T cells (TaKaRa, 632273) using polyethylenimine
596 (PEI) reagent. The 1A-MYO capsid vector allows production of muscle-tropic AAV9 derivative (MyoAAV)
597 [56]. The transfected cells were cultured in the OptiPRO™-SFM medium (Thermo Fisher, 12309019) for 72
598 hours at 37°C to produce virus. Cells and the culture media were collected for AAV purification. AAV
599 particles were extracted with chloroform, precipitated with polyethylene glycol, purified with

600 DNase/RNase digestion followed by chloroform extraction, and concentrated in PBS with Amicon filters
601 (Millipore), as detailed in a previous report [92]. The viral genome copy numbers (vg) were estimated by
602 qPCR using primers amplifying the cTnT promoter region (primer ID KI466 and KI467, **Key Resources**
603 **Table**). MyoAAV particles were administered to mice through retro-orbital venous sinus injection at a
604 dose of 2×10^{11} vg per mouse at 4 weeks of age, which was 14-15 days prior to tamoxifen.
605
606 **Image quantification related to nuclear envelope ruptures**
607 For quantification of nuclei with PCM1-lost nuclear tips and DNA protrusion, we used immunofluorescent
608 images of isolated cardiomyocytes stained for PCM1 and counter-stained with DAPI (DNA) and Phalloidin
609 (F-actin). Rod-shape cardiomyocytes that had a well-defined sarcomere structure based on Phalloidin
610 staining and two or more nuclei were used for quantification. We quantified instances of DAPI signal
611 protrusion from a nuclear envelope site at which PCM1 signals were specifically discontinued ("local
612 PCM1 loss"). The percentage of cells with one or more nuclei with a local PCM1 loss and the number of
613 such nuclei per cell were quantified manually post imaging. We obtained the percentage from >50
614 cardiomyocytes per animal with a total of 3 animals per genotype. The percentages of cardiomyocytes
615 with PCM1-lost nuclei were compared between genotypes using unpaired one-tailed Welch's t-tests in
616 R.
617 For quantification of nuclei with icGAS puncta, we used isolated cardiomyocytes from wild-type
618 or *Lmna*^{CKO} mice treated with MyoAAV-GFP-icGAS. The percentage of cells with icGAS puncta was
619 quantified manually post imaging. We obtained the percentage from >50 cardiomyocytes per animal with
620 a total of 3 animals per genotype. The icGAS-positive cardiomyocyte percentages were compared
621 between genotypes using an unpaired one-tailed Welch's t-test in R.
622 For quantification of NLS-tdTomato intensities, we used *Lmna*$^{F/F}$;*Myh6MCM*$^{Tg/0}$;*Rosa26*$^{CAG\text{-}LSL\text{-}tdTomato/+}$
623 and *Lmna*$^{+/+}$;*Myh6MCM*$^{Tg/0}$;*Rosa26*$^{CAG\text{-}LSL\text{-}tdTomato/+}$ mice. Isolated cardiomyocytes were fixed,
624 immunostained for PCM1, and counterstained with DAPI. Quantification of NLS-tdTomato signals was
625 performed in the Fiji image analysis software. Cardiomyocytes that had two or more nuclei were used for
626 quantification. Nuclei with nuclear envelope ruptures were identified as described above. A freehand-
627 drawn area was placed inside a nucleus for quantification of the nuclear tdTomato signal. A nucleus was
628 selected for quantification using the following algorithm: If a cell had only ruptured nuclei, one ruptured
629 nucleus was randomly selected for quantification; if a cell had both ruptured and unruptured nuclei, one
630 ruptured nucleus was randomly selected for quantification; if a cell had only unruptured nuclei, one
631 unruptured nucleus was randomly selected for quantification. For each nucleus, whether it had a local
632 PCM1 loss with DNA protrusion was manually determined as described above. A second quantification
633 area of the same size as the nuclear area was placed in the cytoplasm for cytoplasmic tdTomato signal
634 quantification. For each of the two areas, a mean NLS-tdTomato pixel intensity was measured using the
635 ROI manager function in Fiji. We performed this quantification process for three mice per genotype. In

636 total, we had quantification information for 99 wild-type cardiomyocytes (all intact PCM1), 90 *Lmna*^{CKO}
637 cardiomyocytes with local PCM1 loss, and 36 *Lmna*^{CKO} cardiomyocytes with intact PCM1. Signal
638 intensities between two groups were compared using Wilcoxon rank sum tests, and P-values were
639 adjusted for multiple testing using the Benjamini-Hochberg procedure in R.
640
641 **TUNEL assay**
642 TUNEL assays were performed on deparaffinized heart sections using a Click-iT™ Plus TUNEL Assay
643 Kits for In Situ Apoptosis Detection (Invitrogen, C10617), according to the manufacturer's instruction. The
644 samples were then co-stained with Alexa Fluor Plus 647 Phalloidin (Invitrogen, A30107) for 1 hour at
645 37°C to visualize cells in tissue sections. For positive controls, sample tissues were treated with DNase
646 I prior to the TUNEL assay. The number of cells with positive staining in the TUNEL assay (TUNEL^{+} cells)
647 was determined using sections from three hearts per genotype. TUNEL positive cells in 2-3 images per
648 mouse (257 x 257 μm^2 per image) were counted manually and compared between two groups using
649 Wilcoxon rank sum tests in R.
650
651 **Immunoblot**
652 Snap-frozen hearts or isolated cardiomyocytes were lysed in the RIPA buffer for cGAS and STING
653 immunoblotting (20 mM Tris-HCl, 150 mM NaCl, 1% IGEPAL, 0.5% sodium deoxycholate, 0.1% SDS, 10
654 mM dithiothreitol, protease and phosphatase inhibitors) or the Urea buffer for Lamin A/C immunoblotting
655 (20 mM HEPES pH 7.4, 1 M NaCl, 8 M urea, protease and phosphatase inhibitors). Proteins were
656 extracted using pestle homogenization and sonication. Cell lysates were centrifuged at 13,000 rpm for 5
657 minutes at 4°C, and proteins in the supernatant were separated by SDS-PAGE. Proteins were transferred
658 to a PVDF membrane. Membranes were blocked with nonfat milk. The primary antibodies were rabbit
659 anti-Lamin A/C antibody (Santa Cruz, sc-20681, 1:1000), rabbit anti-cGAS antibody (Cell Signaling,
660 #31659, 1:500), rabbit anti-STING antibody (Cell Signaling, #13647, 1:500), and rabbit anti-GAPDH
661 antibody (ABclonal, AC001, 1:1000); Secondary antibodies were anti-rabbit or anti-mouse IgG (H+L)
662 DyLight 680 and 800 (Cell Signaling, 1:5000). Signals were detected and quantified in the Odyssey CLx
663 Imager (LI-COR). Gels after protein transfer were counter-stained with Coomassie to evaluate the loaded
664 protein amount.
665
666 **Electron microscopy**
667 Heart tissues were dissected and fixed in 2.5% glutaraldehyde, post-fixed in 1% OsO4 for 1 hour at 4°C,
668 rinsed, dehydrated in ethanol, and infiltrated overnight. The semithin Epon sections were screened by
669 light microscopy to select areas with longitudinal orientation of myocytes that were subsequently
670 processed to prepare thin sections. The sections were stained with 1% uranyl acetate, followed by lead

671 citrate. The sections were imaged using Hitachi Model H-7650 Transmission Electron Microscope at
672 Cincinnati Children's Integrated Pathology Research Facility.
673
674 **Quantitative reverse-transcriptase PCR (RT-PCR)**
675 For RT-PCR analysis, we used wild-type treated with MyoAAV-Luciferase (n=5) or MyoAAV-cGAS (n=3)
676 and *Lmna*^{CKO} mice treated with MyoAAV-Luciferase (n=4) or MyoAAV-cGAS (n=5) at 2 weeks post
677 tamoxifen. Total RNAs of isolated cardiomyocytes were extracted with Trizol LS (Invitrogen, 10296010),
678 treated with DNaseI, and purified. Quantitative RT-PCR was conducted with the Luna Universal One-
679 Step RT-qPCR Kit (NEB, E3005) on a Bio-Rad CFX96 Real-Time PCR Detection System (Bio-Rad) in
680 accordance with the manufacturer's instructions. The primers for mouse genes were: EA096 and EA097
681 for *Cxcl10*; EA098 and EA099 for *Ifnb1*; EA100 and EA101 for *Ifit3*; and KI444 and KI445 for *Actb* (**Key**
682 **Resources Table**). The delta-delta Ct method was used to quantify mRNA abundance with *Actb* as a
683 normalization control. mRNA levels between two groups were compared using Wilcoxon rank sum tests,
684 and P-values were adjusted for multiple testing using the Benjamini-Hochberg procedure in R.
685
686 **RNA-seq**
687 For RNA-seq comparing wild-type mice with *Lmna*^{CKO} mice at different post tamoxifen times, we used
688 wild-type (n=5) and *Lmna*^{CKO} mice (n=4) at 1 week post tamoxifen, wild-type (n=3) and *Lmna*^{CKO} mice
689 (n=2) at 11 days post tamoxifen, and wild-type (n=7) and *Lmna*^{CKO} mice (n=5) at 2 weeks post tamoxifen.
690 For RNA-seq analysis of *Lmna/Cgas* double knockout mice, we used *Cgas*$^{-/-}$;*Lmna*$^{F/F;Myh6MCM}$ mice (n=4),
691 *Cgas*$^{+/+}$;*Lmna*$^{F/F;Myh6MCM}$ (n=6), *Cgas*$^{+/+}$;*Lmna*$^{F/+;Myh6MCM}$ (n=6), and *Cgas*$^{-/-}$;*Lmna*$^{F/+;Myh6MCM}$ (n=4) for
692 experiments. Hearts were perfused with 100 mM KCl and removed for RNA extraction. Total RNAs were
693 extracted with Trizol LS (Invitrogen, 10296010), treated with DNaseI, and purified. For tamoxifen time
694 course experiments, mRNA sequencing libraries were generated using the poly-A selection module in
695 the NEBNext UltraII Directional RNA Library Prep Kit (NEB E7760) and sequenced on the Illumina HiSeq
696 2500 sequencer with single-end 50 cycles. For *cGas*/*Lmna* double knockout experiments, libraries were
697 generated using QuantSeq 3' mRNA-Seq Library Prep Kit FWD (Lexogen, K01596) and sequenced on
698 the Illumina NovaSeq 6000 sequencer with single-end 100 cycles.
699
700 **RNA-seq analysis**
701 High-throughput sequencing reads were aligned to the mouse mm39 reference genome with the
702 Gencode vM27 basic gene annotation using STAR version 2.7.9 [93] with the default alignment parameters
703 except using "clip3pAdapterSeq AGATCGGAAGAGCACACGTCTGAACTCCAGTCA". From raw read
704 counts per transcript, TPMs (transcripts per million) were calculated in R as follows: TPM=10^6 x
705 RPK/sum(RPK), where RPK=read count/transcript length in kp, and sum(RPK) is the sum of RPKs for
706 all transcripts. Raw read counts were used for differential gene expression analyses using DESeq2 [94] in

707 R. Protein-coding or lncRNA genes with adjusted P-value < 0.05 and absolute $\log_2$ fold change > 1 (NEB
708 Directional RNA-seq) or with adjusted P-value < 0.05 and absolute $\log_2$ fold change > 0 (QuantSeq 3'
709 mRNA-seq) were considered differentially expressed genes (**Table S1**). Differentially expressed genes
710 were analyzed for the enrichment of GO Biological Processes, GO Molecular Functions, GO Cellular
711 Components, and KEGG pathway terms using Metascape [95] with the default enrichment parameters.
712
713 **Single-nucleus RNA-seq**
714 For single-nucleus RNA-seq, we used wild-type (n=3) and *Lmna*^{CKO} mice (n=3) at 2 weeks post
715 tamoxifen. Combinatorial indexing-based single-nucleus RNA-seq was conducted according to the
716 optimized sci-RNA-seq3 protocol developed previously [96]. Briefly, mice were anesthetized with
717 isoflurane, euthanized by cervical dislocation, and then hearts were perfused with 100 mM KCl. Removed
718 hearts were diced into small pieces in cold PBS containing Diethyl pyrocarbonate (DEPC, Sigma D5758).
719 Fresh heart pieces were dounce-homogenized to liberate nuclei in Hypotonic lysis buffer B (7.7 mM
720 Na_2HPO_4, 4.5 mM NaH_2PO_4, 1.8 mM KH_2PO_4, 2.7 mM KCl, 10.3 mM NaCl, 3 mM $MgCl_2$, 0.08% BSA,
721 0.025% Igepal CA-630, 1% DEPC) and passed through cell strainers. Nuclei were fixed in 1 mg/mL
722 dithiobis(succinimidyl propionate) (DSP, Thermo Fisher 22585) for 15 min on ice, washed, and stored at
723 –80°C until use. For each mouse, 50,000 nuclei were placed in each of 8 wells of a 96-well plate (total
724 48 wells for 6 mice). The remaining 48 wells were filled with similarly processed mouse heart nuclei with
725 comparable sample quality from an unrelated project. Nuclei were subjected to reverse transcription with
726 96-indexed poly-T RT primers that contained a unique molecular identifier (UMI) sequence
727 (3lvl_mRNA_RT_plate_1; **Table S3**). Nuclei from all wells were combined and redistributed evenly to 96
728 wells. Redistributed cells were subjected to ligation with 96-indexed ligation primers in 96 wells
729 (3lvl_mRNA_Lig_plate_1; **Table S3**). Nuclei from all wells were combined again and redistributed evenly
730 to 96 wells at 1,000 nuclei per well. Redistributed cells underwent second strand synthesis, protease
731 digestion, tagmentation using N7-loaded Tn5 transposase, and PCR-amplified using 96-indexed PCR
732 P7 primers (PCR_P7_plate1; **Table S3**) and the unindexed P5 primer, for 16 cycles. PCR amplicons
733 were combined and size-selected for DNA fragments between 250 bp and 600 bp. Purified library DNA
734 were sequenced for 50 bases on the paired-end mode (34 cycles on Read1 to sequence the ligation
735 index, UMI, and the RT barcode; 10 cycles on Index1 to sequence the P7 index; and 48 cycles on Read2
736 to sequence the cDNA) using an Illumina NovaSeq6000 sequencer.
737
738 **Single-nucleus RNA-seq analysis**
739 Pre-processing of the single-nucleus RNA-seq data was performed using the published sci-RNA-seq3
740 pipeline [96], available in Github (https://github.com/JunyueC/sci-RNA-seq3_pipeline). The sci-RNA-seq3
741 pipeline takes fastq files separated by the P7 index as input, aligns reads to the genome, and returns a
742 gene-by-cell read count matrix. First, raw reads were trimmed to remove poly A tails, aligned to the mm39

743 mouse reference genome using STAR, and filtered for MAPQ greater than or equal to 30. Duplicate reads
744 were removed based on UMI. Read counts per gene were computed for each cell defined by the unique
745 combination of the RT index, ligation index, and P7 index. The gene-by-cell count matrix produced by
746 the sci-RNA-seq3 pipeline was further processed in the *SingleCellExperiment* package framework in R
747 [97]. We used the *scDblFinder* package for doublet detection and the *scuttle* package for mitochondrial
748 RNA quantification in R. We obtained 14,111 nuclei after filtering for nuclei with the *scDblFinder* doublet
749 score less than 0.25 and mitochondrial RNA contamination percentage less than 2% of total RNAs per
750 cell. Read counts for a gene were normalized by per-cell read depth and then log-transformed to obtain
751 normalized expression values ("logcounts"). Logcounts were used to plot expression values in graphs.
752 Principal component analysis (PCA) was performed on logcounts for 2,000 highly variable genes across
753 cells using the *fixedPCA* function in the *scran* package. The top 50 principal components were used in
754 the *runUMAP* function in the *scater* package with n_neighbors=20 and min_dist=1 parameters to obtain
755 UMAP dimensions. To cluster cells, logcounts were processed in the *clusterCells* function in the *scran*
756 package using the top 50 principal components, with the number of nearest neighbors k=12. Cell clusters
757 were annotated manually with cell type names based on marker gene expression. Per-gene read counts
758 were summed within cell groups and processed by the *DESeq2* package [94] to perform pseudo-bulk
759 differential gene expression analysis. Genes with adjusted P-values smaller than 0.05 were defined as
760 differentially expressed genes (**Table S4**). GO analysis of differentially expressed genes was performed
761 as described in the RNA-seq analysis section. For the analysis for the enrichment within selected GO
762 and KEGG terms, all genes associated with the selected terms were obtained using the R packages
763 *GO.db* and *KEGGREST*, and enrichment of differentially expressed genes among these genes was
764 computed by Fisher's exact test with P-values adjusted by the Benjamini-Hochberg procedure. Cell-cell
765 communication analysis was performed using the *CellChat* package in R [74] using the 12 cell type
766 annotations and the default mouse database with a minimum of ten cells for the analysis. Positive
767 communications were selected by the *subsetCommunication* function with threshold P-value less than
768 0.05, and the reported interaction counts were used to plot data.
769
770 **SLAM-IT-seq**
771 For SLAM-IT-seq experiments, we used *Lmna*$^{F/F}$*;Myh6MCM*$^{Tg/0}$*;Uprt*$^{Tg/0}$ (n=6) and
772 *Lmna*$^{+/+}$*;Myh6MCM*$^{Tg/0}$*;Uprt*$^{Tg/0}$ (n=8) mice as experimental groups, and *Lmna*$^{F/F}$*;Myh6MCM*$^{Tg/0}$*;Uprt*$^{0/0}$
773 (n=4) and *Lmna*$^{+/+}$*;Myh6MCM*$^{Tg/0}$*;Uprt*$^{0/0}$ (n=3) mice as negative control groups that would not incorporate
774 4-thiouracil (4sU) due to the absence of the *Uprt* allele. All mice were administered with tamoxifen and
775 used at 2 weeks post tamoxifen treatment. SLAM-IT-seq was conducted according to a previously
776 established protocol [53]. Briefly, mice were intraperitoneally injected with 4-thiouracil (4sU) dissolved in a
777 DMSO/corn oil (1:3) solution at a dose of 10 mg per gram of body weight. Six hours after the injection,
778 mice were sacrificed, and hearts were perfused with 100 mM KCl and removed. RNAs from the left

779 ventricular free wall were extracted by Trizol LS, purified, and DNaseI-treated using Directzol RNA
780 miniprep kit (Zymo, R2052). Purified RNAs (1.5 µg) were subjected to alkylation in the presence of 12
781 mM Iodoacetamide (IAA, Sigma I1149). High-throughput sequencing libraries were generated from the
782 alkylated RNAs using Quant-seq 3' mRNA-seq FWD kit (Lexogen K01596) and sequenced 100 bases
783 on the single-end mode on an Illumina NovaSeq6000 sequencer.
784
785 **SLAM-IT-seq analysis**
786 We analyzed SLAM-IT-seq data according to the published SLAM-IT-seq data analysis pipeline that uses
787 the *slamdunk* package [98], available on GitHub (https://github.com/t-neumann/slamdunk), and R functions
788 [59]. First, raw reads were processed by the *slamdunk all* function in the the *slamdunk* package with the
789 following alignment parameters: --trim-5p 12 --topn 100 --multimap --max-read-length 101 with default --
790 var-fraction (0.8) and default -c (1). This function aligned reads to 3' UTRs of Gencode vM27 genes (total
791 208,307 UTRs from 37,065 unique genes) in the mm39 mouse reference genome. Aligned reads were
792 processed by the *alleyoop utrrates* function in the *slamdunk* package with default parameters to quantify
793 C-to-T conversion events. UTRs with at least one read coverage for all 21 samples were retained for
794 further analyses (47,717 UTRs from 14,250 unique genes). Statistically significant C-to-T conversion
795 events in each transcript (i.e. the likelihood of cardiomyocyte-derived transcripts) were identified by
796 comparing the conversion events in mice carrying the *Uprt* allele with those in mice not carrying this allele
797 using beta-binomial test (*bbtest* function) in R. P-values of the beta binomial test were adjusted with the
798 Benjamini-Hochberg procedure for multiple tests (**Table S2**). A transcript with the lowest adjusted P-
799 value was chosen to represent a gene if there were multiple transcripts per gene. Genes with the adjusted
800 P-values smaller than 0.05 were defined as originating from cardiomyocytes, whereas genes with
801 adjusted P-values greater than or equal to 0.05 were defined as not originating from cardiomyocytes.
802
803 **Quantification and statistical analysis**
804 Statistical details of experiments and sample sizes are described in Method sections and indicated in
805 figures and/or figure legends. Quantitative data were shown as means (bar) of biological replicates (dots).
806 P values < 0.05 were considered statistically significant. P-values are indicated in the figures as
807 appropriate.
808
809 **Image graphics**
810 Graphical abstract and the study summary (**Fig.4J**) were created with BioRender.com.
811
812

REFERENCES

1. Aebi, U., Cohn, J., Buhle, L., and Gerace, L. (1986). The nuclear lamina is a meshwork of intermediate-type filaments. Nature *323*, 560–564.

2. Goldman, A.E., Maul, G., Steinert, P.M., Yang, H.Y., and Goldman, R.D. (1986). Keratin-like proteins that coisolate with intermediate filaments of BHK-21 cells are nuclear lamins. Proc. Natl. Acad. Sci. U. S. A. *83*, 3839–3843.

3. Röber, R.A., Weber, K., and Osborn, M. (1989). Differential timing of nuclear lamin A/C expression in the various organs of the mouse embryo and the young animal: a developmental study. Development *105*, 365–378.

4. Dechat, T., Pfleghaar, K., Sengupta, K., Shimi, T., Shumaker, D.K., Solimando, L., and Goldman, R.D. (2008). Nuclear lamins: major factors in the structural organization and function of the nucleus and chromatin. Genes Dev. *22*, 832–853.

5. Fatkin, D., MacRae, C., Sasaki, T., Wolff, M.R., Porcu, M., Frenneaux, M., Atherton, J., Vidaillet, H.J., Jr, Spudich, S., De Girolami, U., et al. (1999). Missense mutations in the rod domain of the lamin A/C gene as causes of dilated cardiomyopathy and conduction-system disease. N. Engl. J. Med. *341*, 1715–1724.

6. Bonne, G., Di Barletta, M.R., Varnous, S., Bécane, H.M., Hammouda, E.H., Merlini, L., Muntoni, F., Greenberg, C.R., Gary, F., Urtizberea, J.A., et al. (1999). Mutations in the gene encoding lamin A/C cause autosomal dominant Emery-Dreifuss muscular dystrophy. Nat. Genet. *21*, 285–288.

7. Eriksson, M., Brown, W.T., Gordon, L.B., Glynn, M.W., Singer, J., Scott, L., Erdos, M.R., Robbins, C.M., Moses, T.Y., Berglund, P., et al. (2003). Recurrent de novo point mutations in lamin A cause Hutchinson-Gilford progeria syndrome. Nature *423*, 293–298.

8. Chen, L., Lee, L., Kudlow, B.A., Dos Santos, H.G., Sletvold, O., Shafeghati, Y., Botha, E.G., Garg, A., Hanson, N.B., Martin, G.M., et al. (2003). LMNA mutations in atypical Werner's syndrome. Lancet *362*, 440–445.

9. De Sandre-Giovannoli, A., Bernard, R., Cau, P., Navarro, C., Amiel, J., Boccaccio, I., Lyonnet, S., Stewart, C.L., Munnich, A., Le Merrer, M., et al. (2003). Lamin a truncation in Hutchinson-Gilford progeria. Science *300*, 2055–2055.

10. Cao, H., and Hegele, R.A. (2000). Nuclear lamin A/C R482Q mutation in canadian kindreds with Dunnigan-type familial partial lipodystrophy. Hum. Mol. Genet. *9*, 109–112.

11. Parks, S.B., Kushner, J.D., Nauman, D., Burgess, D., Ludwigsen, S., Peterson, A., Li, D., Jakobs, P., Litt, M., Porter, C.B., et al. (2008). Lamin A/C mutation analysis in a cohort of 324 unrelated patients with idiopathic or familial dilated cardiomyopathy. Am. Heart J. *156*, 161–169.

12. Hershberger, R.E., and Morales, A. (2008). LMNA-Related Dilated Cardiomyopathy. In GeneReviews®, M. P. Adam, H. H. Ardinger, R. A. Pagon, S. E. Wallace, L. J. H. Bean, K. Stephens, and A. Amemiya, eds. (University of Washington, Seattle).

13. Taylor, M.R.G., Fain, P.R., Sinagra, G., Robinson, M.L., Robertson, A.D., Carniel, E., Di Lenarda, A., Bohlmeyer, T.J., Ferguson, D.A., Brodsky, G.L., et al. (2003). Natural history of dilated cardiomyopathy due to lamin A/C gene mutations. J. Am. Coll. Cardiol. *41*, 771–780.

14. Sébillon, P., Bouchier, C., Bidot, L.D., Bonne, G., Ahamed, K., Charron, P., Drouin-Garraud, V., Millaire, A., Desrumeaux, G., Benaïche, A., et al. (2003). Expanding the phenotype of LMNA mutations in dilated cardiomyopathy and functional consequences of these mutations. J. Med.

855 Genet. *40*, 560–567.

856 15. van Rijsingen, I.A.W., Nannenberg, E.A., Arbustini, E., Elliott, P.M., Mogensen, J., Hermans-van
857 Ast, J.F., van der Kooi, A.J., van Tintelen, J.P., van den Berg, M.P., Grasso, M., et al. (2013).
858 Gender-specific differences in major cardiac events and mortality in lamin A/C mutation carriers.
859 Eur. J. Heart Fail. *15*, 376–384.

860 16. Charron, P., Arbustini, E., and Bonne, G. (2012). What Should the Cardiologist know about Lamin
861 Disease? Arrhythm Electrophysiol Rev *1*, 22–28.

862 17. Verga, L., Concardi, M., Pilotto, A., Bellini, O., Pasotti, M., Repetto, A., Tavazzi, L., and Arbustini,
863 E. (2003). Loss of lamin A/C expression revealed by immuno-electron microscopy in dilated
864 cardiomyopathy with atrioventricular block caused by LMNA gene defects. Virchows Arch. *443*,
865 664–671.

866 18. Arbustini, E., Pilotto, A., Repetto, A., Grasso, M., Negri, A., Diegoli, M., Campana, C., Scelsi, L.,
867 Baldini, E., Gavazzi, A., et al. (2002). Autosomal dominant dilated cardiomyopathy with
868 atrioventricular block: a lamin A/C defect-related disease. J. Am. Coll. Cardiol. *39*, 981–990.

869 19. Kato, K., Ohno, S., Sonoda, K., Makiyama, T., Ozawa, T., and Horie, M. (2020). Splice site
870 mutation of LMNA causes severe dilated cardiomyopathy via strong dominant reduction of total
871 lamin expression. Eur. Heart J. *41*. 10.1093/ehjci/ehaa946.0333.

872 20. Narula, N., Favalli, V., Tarantino, P., Grasso, M., Pilotto, A., Bellazzi, R., Serio, A., Gambarin, F.I.,
873 Charron, P., Meder, B., et al. (2012). Quantitative expression of the mutated lamin A/C gene in
874 patients with cardiolaminopathy. J. Am. Coll. Cardiol. *60*, 1916–1920.

875 21. Muchir, A., Pavlidis, P., Decostre, V., Herron, A.J., Arimura, T., Bonne, G., and Worman, H.J.
876 (2007). Activation of MAPK pathways links LMNA mutations to cardiomyopathy in Emery-Dreifuss
877 muscular dystrophy. J. Clin. Invest. *117*, 1282–1293.

878 22. Muchir, A., Shan, J., Bonne, G., Lehnart, S.E., and Worman, H.J. (2009). Inhibition of extracellular
879 signal-regulated kinase signaling to prevent cardiomyopathy caused by mutation in the gene
880 encoding A-type lamins. Hum. Mol. Genet. *18*, 241–247.

881 23. Wu, W., Muchir, A., Shan, J., Bonne, G., and Worman, H.J. (2011). Mitogen-Activated Protein
882 Kinase Inhibitors Improve Heart Function and Prevent Fibrosis in Cardiomyopathy Caused by
883 Mutation in Lamin A/C Gene. Circulation *123*, 53–61.

884 24. Muchir, A., Wu, W., Choi, J.C., Iwata, S., Morrow, J., Homma, S., and Worman, H.J. (2012).
885 Abnormal p38α mitogen-activated protein kinase signaling in dilated cardiomyopathy caused by
886 lamin A/C gene mutation. Hum. Mol. Genet. *21*, 4325–4333.

887 25. Choi, J.C., Muchir, A., Wu, W., Iwata, S., Homma, S., Morrow, J.P., and Worman, H.J. (2012).
888 Temsirolimus activates autophagy and ameliorates cardiomyopathy caused by lamin A/C gene
889 mutation. Sci. Transl. Med. *4*, 144ra102.

890 26. Chen, S.N., Lombardi, R., Karmouch, J., Tsai, J.-Y., Czernuszewicz, G., Taylor, M.R.G., Mestroni,
891 L., Coarfa, C., Gurha, P., and Marian, A.J. (2019). DNA Damage Response/TP53 Pathway Is
892 Activated and Contributes to the Pathogenesis of Dilated Cardiomyopathy Associated With LMNA
893 (Lamin A/C) Mutations. Circ. Res. *124*, 856–873.

894 27. Cheedipudi, S.M., Asghar, S., and Marian, A.J. (2022). Genetic Ablation of the DNA Damage
895 Response Pathway Attenuates Lamin-Associated Dilated Cardiomyopathy in Mice. JACC Basic
896 Transl Sci *7*, 1232–1245.

897 28. Davidson, P.M., and Lammerding, J. (2014). Broken nuclei--lamins, nuclear mechanics, and
898 disease. Trends Cell Biol. *24*, 247–256.

899 29. Chen, N.Y., Yang, Y., Weston, T.A., Belling, J.N., Heizer, P., Tu, Y., Kim, P., Edillo, L., Jonas, S.J.,
900 Weiss, P.S., et al. (2019). An absence of lamin B1 in migrating neurons causes nuclear membrane
901 ruptures and cell death. Proc. Natl. Acad. Sci. U. S. A. *116*, 25870–25879.

902 30. Cho, S., Vashisth, M., Abbas, A., Majkut, S., Vogel, K., Xia, Y., Ivanovska, I.L., Irianto, J., Tewari,
903 M., Zhu, K., et al. (2019). Mechanosensing by the Lamina Protects against Nuclear Rupture, DNA
904 Damage, and Cell-Cycle Arrest. Dev. Cell *49*, 920-935.e5.

905 31. Earle, A.J., Kirby, T.J., Fedorchak, G.R., Isermann, P., Patel, J., Iruvanti, S., Moore, S.A., Bonne,
906 G., Wallrath, L.L., and Lammerding, J. (2020). Mutant lamins cause nuclear envelope rupture and
907 DNA damage in skeletal muscle cells. Nat. Mater. *19*, 464–473.

908 32. Sylvius, N., Bilinska, Z.T., Veinot, J.P., Fidzianska, A., Bolongo, P.M., Poon, S., McKeown, P.,
909 Davies, R.A., Chan, K.-L., Tang, A.S.L., et al. (2005). In vivo and in vitro examination of the
910 functional significances of novel lamin gene mutations in heart failure patients. J. Med. Genet. *42*,
911 639–647.

912 33. Hatch, E.M., and Hetzer, M.W. (2016). Nuclear envelope rupture is induced by actin-based nucleus
913 confinement. J. Cell Biol. *215*, 27–36.

914 34. Vargas, J.D., Hatch, E.M., Anderson, D.J., and Hetzer, M.W. (2012). Transient nuclear envelope
915 rupturing during interphase in human cancer cells. Nucleus *3*, 88–100.

916 35. De Vos, W.H., Houben, F., Kamps, M., Malhas, A., Verheyen, F., Cox, J., Manders, E.M.M.,
917 Verstraeten, V.L.R.M., van Steensel, M.A.M., Marcelis, C.L.M., et al. (2011). Repetitive disruptions
918 of the nuclear envelope invoke temporary loss of cellular compartmentalization in laminopathies.
919 Hum. Mol. Genet. *20*, 4175–4186.

920 36. Siu, C.-W., Lee, Y.-K., Ho, J.C.-Y., Lai, W.-H., Chan, Y.-C., Ng, K.-M., Wong, L.-Y., Au, K.-W., Lau,
921 Y.-M., Zhang, J., et al. (2012). Modeling of lamin A/C mutation premature cardiac aging using
922 patient-specific induced pluripotent stem cells. Aging *4*, 803–822.

923 37. Fan, Y., Tan, D., Zhang, X., Song, D., Chang, X., Wang, S., Yan, H., Ge, L., Yang, H.,
924 Bönnemann, C., et al. (2020). Nuclear Factor-κB Pathway Mediates the Molecular Pathogenesis of
925 LMNA-Related Muscular Dystrophies. Biochem. Genet. *58*, 966–980.

926 38. Chai, R.J., Werner, H., Li, P.Y., Lee, Y.L., Nyein, K.T., Solovei, I., Luu, T.D.A., Sharma, B.,
927 Navasankari, R., Maric, M., et al. (2021). Disrupting the LINC complex by AAV mediated gene
928 transduction prevents progression of Lamin induced cardiomyopathy. Nat. Commun. *12*, 4722.

929 39. Chen, R., Buchmann, S., Kroth, A., Arias-Loza, A.-P., Kohlhaas, M., Wagner, N., Grüner, G.,
930 Nickel, A., Cirnu, A., Williams, T., et al. (2023). Mechanistic Insights of the LEMD2 p.L13R
931 Mutation and Its Role in Cardiomyopathy. Circ. Res. *132*, e43–e58.

932 40. Kim, P.H., Chen, N.Y., Heizer, P.J., Tu, Y., Weston, T.A., Fong, J.L.-C., Gill, N.K., Rowat, A.C.,
933 Young, S.G., and Fong, L.G. (2021). Nuclear membrane ruptures underlie the vascular pathology
934 in a mouse model of Hutchinson-Gilford progeria syndrome. JCI Insight *6*.
935 10.1172/jci.insight.151515.

936 41. Ross, J.A., Arcos-Villacis, N., Battey, E., Boogerd, C., Avalos Orellana, C., Marhuenda, E.,
937 Swiatlowska, P., Hodzic, D., Prin, F., Mohun, T., et al. (2023). Lem2 is essential for cardiac
938 development by maintaining nuclear integrity. Cardiovasc. Res. 10.1093/cvr/cvad061.

939 42. Zhang, Y., Ramirez-Martinez, A., Chen, K., McAnally, J.R., Cai, C., Durbacz, M.Z., Chemello, F.,
940 Wang, Z., Xu, L., Bassel-Duby, R., et al. (2023). Net39 protects muscle nuclei from mechanical
941 stress during the pathogenesis of Emery-Dreifuss muscular dystrophy. J. Clin. Invest. *133*.
942 10.1172/JCI163333.

943 43. Eissenberg, J.C., and Gonzalo, S. (2020). Pushing the limit on laminopathies. Nat. Mater. *19*, 378–
944 380.

945 44. Gauthier, B.R., and Comaills, V. (2021). Nuclear Envelope Integrity in Health and Disease:
946 Consequences on Genome Instability and Inflammation. Int. J. Mol. Sci. *22*.
947 10.3390/ijms22147281.

948 45. Miller, K.N., Victorelli, S.G., Salmonowicz, H., Dasgupta, N., Liu, T., Passos, J.F., and Adams, P.D.
949 (2021). Cytoplasmic DNA: sources, sensing, and role in aging and disease. Cell *184*, 5506–5526.

950 46. Yum, S., Li, M., Fang, Y., and Chen, Z.J. (2021). TBK1 recruitment to STING activates both IRF3
951 and NF-κB that mediate immune defense against tumors and viral infections. Proceedings of the
952 National Academy of Sciences *118*, e2100225118.

953 47. Decout, A., Katz, J.D., Venkatraman, S., and Ablasser, A. (2021). The cGAS–STING pathway as a
954 therapeutic target in inflammatory diseases. Nat. Rev. Immunol. *21*, 548–569.

955 48. Kreienkamp, R., Graziano, S., Coll-Bonfill, N., Bedia-Diaz, G., Cybulla, E., Vindigni, A., Dorsett, D.,
956 Kubben, N., Batista, L.F.Z., and Gonzalo, S. (2018). A Cell-Intrinsic Interferon-like Response Links
957 Replication Stress to Cellular Aging Caused by Progerin. Cell Rep. *22*, 2006–2015.

958 49. King, K.R., Aguirre, A.D., Ye, Y.-X., Sun, Y., Roh, J.D., Ng, R.P., Jr, Kohler, R.H., Arlauckas, S.P.,
959 Iwamoto, Y., Savol, A., et al. (2017). IRF3 and type I interferons fuel a fatal response to myocardial
960 infarction. Nat. Med. *23*, 1481–1487.

961 50. Cao, D.J., Schiattarella, G.G., Villalobos, E., Jiang, N., May, H.I., Li, T., Chen, Z.J., Gillette, T.G.,
962 and Hill, J.A. (2018). Cytosolic DNA Sensing Promotes Macrophage Transformation and Governs
963 Myocardial Ischemic Injury. Circulation *137*, 2613–2634.

964 51. Hu, D., Cui, Y.-X., Wu, M.-Y., Li, L., Su, L.-N., Lian, Z., and Chen, H. (2020). Cytosolic DNA sensor
965 cGAS plays an essential pathogenetic role in pressure overload-induced heart failure. Am. J.
966 Physiol. Heart Circ. Physiol. *318*, H1525–H1537.

967 52. Yan, M., Li, Y., Luo, Q., Zeng, W., Shao, X., Li, L., Wang, Q., Wang, D., Zhang, Y., Diao, H., et al.
968 (2022). Mitochondrial damage and activation of the cytosolic DNA sensor cGAS-STING pathway
969 lead to cardiac pyroptosis and hypertrophy in diabetic cardiomyopathy mice. Cell Death Discov *8*,
970 258.

971 53. Hasper, J., Welle, K., Swovick, K., Hryhorenko, J., Ghaemmaghami, S., and Buchwalter, A. (2024).
972 Long lifetime and tissue-specific accumulation of lamin A/C in Hutchinson-Gilford progeria
973 syndrome. J. Cell Biol. *223*. 10.1083/jcb.202307049.

974 54. Patterson, M., Barske, L., Van Handel, B., Rau, C.D., Gan, P., Sharma, A., Parikh, S., Denholtz,
975 M., Huang, Y., Yamaguchi, Y., et al. (2017). Frequency of mononuclear diploid cardiomyocytes
976 underlies natural variation in heart regeneration. Nat. Genet. *49*, 1346–1353.

977 55. Srsen, V., Fant, X., Heald, R., Rabouille, C., and Merdes, A. (2009). Centrosome proteins form an
978 insoluble perinuclear matrix during muscle cell differentiation. BMC Cell Biol. *10*, 28.

979 56. Tabebordbar, M., Lagerborg, K.A., Stanton, A., King, E.M., Ye, S., Tellez, L., Krunnfusz, A.,

980 Tavakoli, S., Widrick, J.J., Messemer, K.A., et al. (2021). Directed evolution of a family of AAV
981 capsid variants enabling potent muscle-directed gene delivery across species. Cell *184*, 4919-
982 4938.e22.

983 57. Denais, C.M., Gilbert, R.M., Isermann, P., McGregor, A.L., te Lindert, M., Weigelin, B., Davidson,
984 P.M., Friedl, P., Wolf, K., and Lammerding, J. (2016). Nuclear envelope rupture and repair during
985 cancer cell migration. Science *352*, 353–358.

986 58. Raab, M., Gentili, M., de Belly, H., Thiam, H.R., Vargas, P., Jimenez, A.J., Lautenschlaeger, F.,
987 Voituriez, R., Lennon-Duménil, A.M., Manel, N., et al. (2016). ESCRT III repairs nuclear envelope
988 ruptures during cell migration to limit DNA damage and cell death. Science *352*, 359–362.

989 59. Matsushima, W., Herzog, V.A., Neumann, T., Gapp, K., Zuber, J., Ameres, S.L., and Miska, E.A.
990 (2019). Sequencing cell-type-specific transcriptomes with SLAM-ITseq. Nat. Protoc. *14*, 2261–
991 2278.

992 60. Kuhl, N., Linder, A., Philipp, N., Nixdorf, D., Fischer, H., Veth, S., Kuut, G., Xu, T.T., Theurich, S.,
993 Carell, T., et al. (2023). STING agonism turns human T cells into interferon-producing cells but
994 impedes their functionality. EMBO Rep. *24*, e55536.

995 61. Liu, Y., Xu, P., Rivara, S., Liu, C., Ricci, J., Ren, X., Hurley, J.H., and Ablasser, A. (2022). Clathrin-
996 associated AP-1 controls termination of STING signalling. Nature *610*, 761–767.

997 62. Ikushima, H., Negishi, H., and Taniguchi, T. (2013). The IRF family transcription factors at the
998 interface of innate and adaptive immune responses. Cold Spring Harb. Symp. Quant. Biol. *78*,
999 105–116.

1000 63. Della Corte, C.M., Sen, T., Gay, C.M., Ramkumar, K., Diao, L., Cardnell, R.J., Rodriguez, B.L.,
1001 Stewart, C.A., Papadimitrakopoulou, V.A., Gibson, L., et al. (2020). STING Pathway Expression
1002 Identifies NSCLC With an Immune-Responsive Phenotype. J. Thorac. Oncol. *15*, 777–791.

1003 64. Schoggins, J.W., MacDuff, D.A., Imanaka, N., Gainey, M.D., Shrestha, B., Eitson, J.L., Mar, K.B.,
1004 Richardson, R.B., Ratushny, A.V., Litvak, V., et al. (2014). Pan-viral specificity of IFN-induced
1005 genes reveals new roles for cGAS in innate immunity. Nature *505*, 691–695.

1006 65. Jin, L., Hill, K.K., Filak, H., Mogan, J., Knowles, H., Zhang, B., Perraud, A.-L., Cambier, J.C., and
1007 Lenz, L.L. (2011). MPYS is required for IFN response factor 3 activation and type I IFN production
1008 in the response of cultured phagocytes to bacterial second messengers cyclic-di-AMP and cyclic-
1009 di-GMP. J. Immunol. *187*, 2595–2601.

1010 66. Cohen, T.V., Gnocchi, V.F., Cohen, J.E., Phadke, A., Liu, H., Ellis, J.A., Foisner, R., Stewart, C.L.,
1011 Zammit, P.S., and Partridge, T.A. (2013). Defective skeletal muscle growth in lamin A/C-deficient
1012 mice is rescued by loss of Lap2α. Hum. Mol. Genet. *22*, 2852–2869.

1013 67. Ortega, A., Roselló-Lletí, E., Tarazón, E., Molina-Navarro, M.M., Martínez-Dolz, L., González-
1014 Juanatey, J.R., Lago, F., Montoro-Mateos, J.D., Salvador, A., Rivera, M., et al. (2014).
1015 Endoplasmic reticulum stress induces different molecular structural alterations in human dilated
1016 and ischemic cardiomyopathy. PLoS One *9*, e107635.

1017 68. Sasagawa, S., Nishimura, Y., Okabe, S., Murakami, S., Ashikawa, Y., Yuge, M., Kawaguchi, K.,
1018 Kawase, R., Okamoto, R., Ito, M., et al. (2016). Downregulation of GSTK1 Is a Common
1019 Mechanism Underlying Hypertrophic Cardiomyopathy. Front. Pharmacol. *7*, 162.

1020 69. Fan, P., Zhang, L., Cheng, T., Wang, J., Zhou, J., Zhao, L., Hua, C., and Xia, Q. (2021). MiR-590-
1021 5p inhibits pathological hypertrophy mediated heart failure by targeting RTN4. J. Mol. Histol. *52*,

1022 955–964.

1023 70. Wehrens, M., de Leeuw, A.E., Wright-Clark, M., Eding, J.E.C., Boogerd, C.J., Molenaar, B., van
1024 der Kraak, P.H., Kuster, D.W.D., van der Velden, J., Michels, M., et al. (2022). Single-cell
1025 transcriptomics provides insights into hypertrophic cardiomyopathy. Cell Rep. *39*, 110809.

1026 71. Snider, P., Standley, K.N., Wang, J., Azhar, M., Doetschman, T., and Conway, S.J. (2009). Origin
1027 of cardiac fibroblasts and the role of periostin. Circ. Res. *105*, 934–947.

1028 72. Lavine, K.J., Epelman, S., Uchida, K., Weber, K.J., Nichols, C.G., Schilling, J.D., Ornitz, D.M.,
1029 Randolph, G.J., and Mann, D.L. (2014). Distinct macrophage lineages contribute to disparate
1030 patterns of cardiac recovery and remodeling in the neonatal and adult heart. Proc. Natl. Acad. Sci.
1031 U. S. A. *111*, 16029–16034.

1032 73. Liu, C., Raab, M., Gui, Y., and Rudd, C.E. (2023). Multi-functional adaptor SKAP1: regulator of
1033 integrin activation, the stop-signal, and the proliferation of T cells. Front. Immunol. *14*, 1192838.

1034 74. Jin, S., Guerrero-Juarez, C.F., Zhang, L., Chang, I., Ramos, R., Kuan, C.-H., Myung, P., Plikus,
1035 M.V., and Nie, Q. (2021). Inference and analysis of cell-cell communication using CellChat. Nat.
1036 Commun. *12*, 1088.

1037 75. Zhang, H., Ren, L., and Wu, J.C. (2022). New Insights Into the Therapy for Lamin-Associated
1038 Dilated Cardiomyopathy. JACC Basic Transl Sci *7*, 1246–1248.

1039 76. Long, Z.-J., Wang, J.-D., Xu, J.-Q., Lei, X.-X., and Liu, Q. (2022). cGAS/STING cross-talks with cell
1040 cycle and potentiates cancer immunotherapy. Mol. Ther. *30*, 1006–1017.

1041 77. Yang, H., Wang, H., Ren, J., Chen, Q., and Chen, Z.J. (2017). cGAS is essential for cellular
1042 senescence. Proc. Natl. Acad. Sci. U. S. A. *114*, E4612–E4620.

1043 78. Thomsen, M.K., Nandakumar, R., Stadler, D., Malo, A., Valls, R.M., Wang, F., Reinert, L.S.,
1044 Dagnaes-Hansen, F., Hollensen, A.K., Mikkelsen, J.G., et al. (2016). Lack of immunological DNA
1045 sensing in hepatocytes facilitates hepatitis B virus infection. Hepatology *64*, 746–759.

1046 79. Li, T., and Chen, Z.J. (2018). The cGAS-cGAMP-STING pathway connects DNA damage to
1047 inflammation, senescence, and cancer. J. Exp. Med. *215*, 1287–1299.

1048 80. Willaume, S., Rass, E., Fontanilla-Ramirez, P., Moussa, A., Wanschoor, P., and Bertrand, P.
1049 (2021). A Link between Replicative Stress, Lamin Proteins, and Inflammation. Genes *12*.
1050 10.3390/genes12040552.

1051 81. Rouhi, L., Auguste, G., Zhou, Q., Lombardi, R., Olcum, M., Pourebrahim, K., Cheedipudi, S.M.,
1052 Asghar, S., Hong, K., Robertson, M.J., et al. (2022). Deletion of the Lmna gene in fibroblasts
1053 causes senescence-associated dilated cardiomyopathy by activating the double-stranded DNA
1054 damage response and induction of senescence-associated secretory phenotype. J Cardiovasc
1055 Aging *2*. 10.20517/jca.2022.14.

1056 82. Liu, Y., Chen, X., Zhao, Y., Wang, X.-Y., Luo, Y.-W., Chen, L., Wang, W., Zhong, S., Hu, M., Dai,
1057 Z., et al. (2023). Small cytosolic double-stranded DNA represses cyclic GMP-AMP synthase
1058 activation and induces autophagy. Cell Rep. *42*, 112852.

1059 83. Nader, G.P. de F., Agüera-Gonzalez, S., Routet, F., Gratia, M., Maurin, M., Cancila, V., Cadart, C.,
1060 Palamidessi, A., Ramos, R.N., San Roman, M., et al. (2021). Compromised nuclear envelope
1061 integrity drives TREX1-dependent DNA damage and tumor cell invasion. Cell *184*, 5230-5246.e22.

1062 84. Kim, Y., and Zheng, Y. (2013). Generation and characterization of a conditional deletion allele for

1063 Lmna in mice. Biochem. Biophys. Res. Commun. *440*, 8–13.

1064 85. Sohal, D.S., Nghiem, M., Crackower, M.A., Witt, S.A., Kimball, T.R., Tymitz, K.M., Penninger, J.M.,
1065 and Molkentin, J.D. (2001). Temporally regulated and tissue-specific gene manipulations in the
1066 adult and embryonic heart using a tamoxifen-inducible Cre protein. Circ. Res. *89*, 20–25.

1067 86. Daigle, T.L., Madisen, L., Hage, T.A., Valley, M.T., Knoblich, U., Larsen, R.S., Takeno, M.M.,
1068 Huang, L., Gu, H., Larsen, R., et al. (2018). A Suite of Transgenic Driver and Reporter Mouse
1069 Lines with Enhanced Brain-Cell-Type Targeting and Functionality. Cell *174*, 465-480.e22.

1070 87. Gay, L., Miller, M.R., Ventura, P.B., Devasthali, V., Vue, Z., Thompson, H.L., Temple, S., Zong, H.,
1071 Cleary, M.D., Stankunas, K., et al. (2013). Mouse TU tagging: a chemical/genetic intersectional
1072 method for purifying cell type-specific nascent RNA. Genes Dev. *27*, 98–115.

1073 88. Verzi, M.P., McCulley, D.J., De Val, S., Dodou, E., and Black, B.L. (2005). The right ventricle,
1074 outflow tract, and ventricular septum comprise a restricted expression domain within the
1075 secondary/anterior heart field. Dev. Biol. *287*, 134–145.

1076 89. Lin, Z., von Gise, A., Zhou, P., Gu, F., Ma, Q., Jiang, J., Yau, A.L., Buck, J.N., Gouin, K.A., van
1077 Gorp, P.R.R., et al. (2014). Cardiac-specific YAP activation improves cardiac function and survival
1078 in an experimental murine MI model. Circ. Res. *115*, 354–363.

1079 90. Chen, X., Zaro, J.L., and Shen, W.-C. (2013). Fusion protein linkers: property, design and
1080 functionality. Adv. Drug Deliv. Rev. *65*, 1357–1369.

1081 91. Sancak, Y., Peterson, T.R., Shaul, Y.D., Lindquist, R.A., Thoreen, C.C., Bar-Peled, L., and
1082 Sabatini, D.M. (2008). The Rag GTPases bind raptor and mediate amino acid signaling to
1083 mTORC1. Science *320*, 1496–1501.

1084 92. Negrini, M., Wang, G., Heuer, A., Björklund, T., and Davidsson, M. (2020). AAV Production
1085 Everywhere: A Simple, Fast, and Reliable Protocol for In-house AAV Vector Production Based on
1086 Chloroform Extraction. Curr. Protoc. Neurosci. *93*, e103.

1087 93. Frankish, A., Diekhans, M., Jungreis, I., Lagarde, J., Loveland, J.E., Mudge, J.M., Sisu, C., Wright,
1088 J.C., Armstrong, J., Barnes, I., et al. (2021). GENCODE 2021. Nucleic Acids Res. *49*, D916–D923.

1089 94. Love, M.I., Huber, W., and Anders, S. (2014). Moderated estimation of fold change and dispersion
1090 for RNA-seq data with DESeq2. Genome Biol. *15*, 550.

1091 95. Zhou, Y., Zhou, B., Pache, L., Chang, M., Khodabakhshi, A.H., Tanaseichuk, O., Benner, C., and
1092 Chanda, S.K. (2019). Metascape provides a biologist-oriented resource for the analysis of
1093 systems-level datasets. Nat. Commun. *10*, 1523.

1094 96. Martin, B.K., Qiu, C., Nichols, E., Phung, M., Green-Gladden, R., Srivatsan, S., Blecher-Gonen, R.,
1095 Beliveau, B.J., Trapnell, C., Cao, J., et al. (2022). Optimized single-nucleus transcriptional profiling
1096 by combinatorial indexing. Nat. Protoc. 10.1038/s41596-022-00752-0.

1097 97. Amezquita, R.A., Lun, A.T.L., Becht, E., Carey, V.J., Carpp, L.N., Geistlinger, L., Marini, F., Rue-
1098 Albrecht, K., Risso, D., Soneson, C., et al. (2020). Orchestrating single-cell analysis with
1099 Bioconductor. Nat. Methods *17*, 137–145.

1100 98. Herzog, V.A., Reichholf, B., Neumann, T., Rescheneder, P., Bhat, P., Burkard, T.R., Wlotzka, W.,
1101 von Haeseler, A., Zuber, J., and Ameres, S.L. (2017). Thiol-linked alkylation of RNA to assess
1102 expression dynamics. Nat. Methods *14*, 1198–1204.

1103

1104 **Key resources table**

REAGENT or RESOURCE	SOURCE	IDENTIFIER
Antibodies		
Anti-Lamin A/C	Abcam	Cat # Ab26300
Anti-Lamin A/C	Santa Cruz	Cat # sc-376248
Anti-Lamin A/C	Santa Cruz	Cat # sc-20681
Anti-CD45 antibody	R&D Systems	Cat # AF114-SP
Anti-CD68 antibody	Cell Signaling	Cat # 97778
Anti-γ-H2A.X antibody	Cell Signaling	Cat # 9718
Anti-desmin antibody	Invitrogen	Cat # PA5-19063
Anti-PCM-1 antibody	Sigma	Cat # HPA023370
Anti-tdTomato antibody	OriGene	Cat # AB8181
Anti-COX4 antibody	R&D Systems	Cat # MAB6980
Anti-cGAS antibody	Cell Signaling	Cat # 31659
Anti-STING antibody	Cell Signaling	Cat # 13647
Anti-GAPDH antibody	ABclonal	Cat # AC001
Alexa Fluor Plus 647 Phalloidin	ThermoFisher	Cat # A30107
Bacterial and virus strains		
Chemicals, peptides, and recombinant proteins		
Tamoxifen	Sigma	Cat # T5648
Collagenase Type II	Worthington	Cat # LS004177
Polyethylenimine, Linear, MW 25000, Transfection Grade (PEI 25K™)	Fisher Scientific	Cat # 23966-100
Target Retrieval Solution	DAKO	Cat # S2367
Corn oil	Sigma	Cat # C8267
Phenol/Chloroform/Isoamyl alcohol	Invitrogen	Cat # 15593031
Trizol LS	Invitrogen	Cat # 10296010
Heparin	Sagent Pharmaceuticals.	Cat # 25021-400-10
VectaStain ELITE ABC Kits	Vector Laboratories	Cat # PK-6100
DAB	DAKO	Cat # K3468
ProLong Glass Antifade Mountant	Invitrogen	Cat # P36984
Normal donkey serum	Jackson ImmunoResearch	Cat # 017-000-121
Sudan Black B	Electron Microscopy Slides	Cat # 21610
NEBuilder HiFi DNA Assembly Master Mix	NEB	Cat # E2621
Dulbecco's modified Eagle medium	Fisher Scientific	Cat # 11965-092
penicillin/streptomycin	Invitrogen	Cat # 105727
OptiPRO™-SFM	Thermo Fisher	Cat # 12309019
Fetal Bovine Serum	Sigma	Cat # F1051
Critical commercial assays		
Masson's Trichrome Kit	Thomas Scientific LLC	Cat # KTMTRPT
Click-iT™ Plus TUNEL Assay Kits for In Situ Apoptosis Detection; Alexa Fluor™ 488	Invitrogen	Cat # C10617
Luna Universal One-Step RT-qPCR Kit	New England Biolabs	Cat # E3005
NEBNext UltraII Directional RNA Library Prep Kit	New England Biolabs	Cat # E7760
Quant-seq 3' mRNA-seq FWD kit	Lexogen	Cat # K01596
Deposited data		

Experimental models: Organisms/strains		
Lmna-LoxP mice	Jackson Laboratory	JAX stock No: 26284
Myh6-MerCreMer transgene mice	Jackson Laboratory	JAX stock No: 005657
Rosa26$^{CAG\text{-}LSL\text{-}tdTomato}$ mice	Jackson Laboratory	JAX stock No: 25106
Cgas-null mice	Jackson Laboratory	JAX stock No: 026554
CAG-Lox-Stop-Lox-Uprt transgene mice	Jackson Laboratory	JAX stock No: 021469
Sting-flox mice	Jackson Laboratory	JAX stock No: 031670
Mice carrying the *Mef2C-AHF-Cre* transgene allele	Verzi *et al*., 2005	DOI: 10.1016/j.ydbio.2005.08.041
Sting-null (generated from *Sting-LoxP* mouse)	This study	N/A
AAVpro 293T Cell	TaKaRa	Cat # 632273
Oligonucleotides		
DNA oligonucleotide KI279 for *Lmna* genotype primer: AACCCAGCCTCAGAAACTGGTGGATG	This paper	Ikegami lab ID: KI279
DNA oligonucleotide KI280 for *Lmna* genotype primer: GACAGCTCTCCTCTGAAGTGCTTGGA	This paper	Ikegami lab ID: Ki280
DNA oligonucleotide EA062 for EGFP cloning: AGTACTTAATACGACTCACTATAGGCTAGCGCCACCATGGTGAGCAAGGGCGAGGA	This paper	Ikegami lab ID: EA062
DNA oligonucleotide EA064 for EGFP with GS linker cloning: TTATCATGTCTGGATCCGCGCGGCCGCGCTGCCCCCGCCTCCCTTGTACAGCTCGTCCATGC	This paper	Ikegami lab ID: EA064

DNA oligonucleotide EA086 for icGAS (human cGAS with E225A/D227A amino acid substitutions): AAGGGAGGCGGGGGCAGCGCGGCCGCAGACTACAAAGACGAT GACGACAAGATGCAGCCCTGGCACGGTAAAGCAATGCAACGGG CTAGTGAAGCAGGAGCTACTGCTCCAAAGGCCAGTGCTAGGAAT GCCAGGGGCGCTCCCATGGATCCAAATGAAAGCCCCGCAGCACC CGAAGCAGCTCTGCCTAAAGCAGGTAAGTTTGGCCCTGCTCGGA AGTCTGGTTCCAGACAAAAGAAATCAGCTCCTGATACTCAAGAG AGGCCTCCAGTAAGGGCTACCGGAGCTAGGGCCAAGAAAGCAC CCCAGAGAGCCCAGGATACCCAGCCTAGTGATGCAACTTCAGCC CCAGGCGCAGAGGGGCTGGAACCTCCCGCCGCACGAGAGCCCG CCCTTTCACGAGCCGGATCCTGCCGCCAACGAGGTGCCAGATGC AGCACAAAACCCAGGCCCCCTCCCGGTCCATGGGATGTACCCAG CCCCGGTCTTCCCGTAAGTGCACCAATATTGGTTCGAAGGGACG CCGCACCAGGGGCCTCTAAACTGCGGGCCGTGCTGGAGAAGCT GAAGTTGTCTCGGGATGATATCAGCACTGCCGCTGGCATGGTTA AAGGGGTTGTTGACCATCTGCTTCTGCGACTGAAATGCGACTCA GCTTTTAGGGGTGTAGGGCTTCTGAACACTGGATCCTATTACGA GCACGTCAAGATTAGTGCTCCCAACGCCTTCGCAGTCATGTTTAA GCTGGAAGTTCCTAGAATTCAGCTGGAAGAGTATTCTAACACTCG AGCTTATTATTTTGTCAAATTTAAGCGAAACCCAAAGGAGAATCA CCTGTCTCAGTTCTTGGAAGGGGAGATACTGTCCGCCTCTAAGAT GCTGTCTAAGTTCAGAAAGATTATAAAGGAGGAAATTAATGATA TCAAAGATACTGACGTGATTATGAAAAGGAAGCGCGGAGGTTCT CCTGCAGTGACTCTGCTCATTAGCGAGAAGATATCTGTTGACATA ACCCTCGCACTCGAATCCAAGTCTAGCTGGCCTGCCTCTACCCAG GAGGGCTTGAGAATTCAAAACTGGTTGTCTGCAAAAGTAAGGAA ACAACTTCGACTGAAGCCATTTTATCTCGTCCCAAAGCACGCAAA AGAGGGCAATGGTTTCCAAGAAGAAACTTGGCGCTTGTCCTTTTC ACACATTGAGAAGGAGATTCTGAACAATCACGGAAAGTCCAAAA CTTGCTGCGAGAATAAGGAAGAAAAGTGCTGTCGAAAGGACTG CTTGAAGTTGATGAAGTATCTCCTGGAACAGTTGAAGGAACGAT TTAAAGATAAGAAACACTTGGACAAATTTAGTTCCTACCACGTGA AGACAGCCTTCTTTCACGTGTGTACCCAGAATCCCCAGGATTCAC AGTGGGATAGAAAGGACCTCGGACTCTGCTTTGACAATTGCGTC ACTTATTTTCTTCAGTGTTTGCGAACTGAGAAGCTGGAAAACTAT TTTATCCCCGAATTTAATTTGTTCTCATCAAACCTGATTGACAAGA GATCTAAAGAATTCCTCACAAAACAGATCGAGTACGAACGCAAC AACGAATTCCCCGTCTTTGATGAATTTTGAGCGGCCGCGCGGATC CAGACATGATAA	This paper	Ikegami lab ID: EA086

DNA oligonucleotide EA087 for mouse cGAS: AGTACTTAATACGACTCACTATAGGCTAGCGCCACCATGGACTAC AAAGACGATGACGATAAGATGGAGGATCCTCGCAGGCGCACCA CAGCTCCACGCGCAAAGAAACCATCTGCTAAGAGAGCACCTACC CAGCCTTCTAGGACAAGAGCCCATGCCGAGTCCTGCGGACCACA ACGAGGCGCCAGGAGTCGGCGGGCAGAACGGGACGGAGACAC AACCGAGAAACCTAGGGCTCCTGGCCCTAGAGTGCACCCAGCAC GCGCTACAGAGCTGACTAAAGATGCACAGCCCAGTGCAATGGAT GCAGCTGGTGCCACCGCACGCCCAGCCGTGCGGGTTCCACAACA GCAGGCTATATTGGACCCCGAACTTCCTGCTGTAAGGGAACCTCA ACCCCCCGCAGATCCCGAAGCTAGAAAAGTAGTACGAGGACCTT CTCACCGACGAGGGGCTCGATCAACCGGCCAGCCACGGGCTCCC AGGGGGTCACGCAAAGAACCAGATAAGCTCAAGAAAGTCCTGG ATAAGTTGCGGTTGAAAAGAAAAGACATCAGTGAAGCTGCTGAA ACAGTTAACAAAGTCGTCGAGAGACTGTTGCGGCGCATGCAAAA AAGGGAATCTGAATTCAAAGGAGTCGAACAACTCAACACCGGTT CATACTACGAGCATGTTAAAATCTCAGCCCCAAATGAGTTTGATG TGATGTTTAAGCTTGAAGTGCCTCGCATTGAACTGCAGGAGTACT ATGAGACTGGAGCCTTTTACCTCGTAAAGTTTAAGCGAATTCCTA GGGGTAATCCCTTGTCTCATTTTCTCGAAGGTGAAGTCTTGTCAG CTACCAAAATGCTGAGTAAATTTAGGAAGATAATAAAAGAGGAG GTTAAGGAAATAAAGGACATCGACGTTTCAGTGGAGAAGGAGA AGCCCGGTTCTCCAGCAGTTACACTCCTCATCAGGAATCCCGAGG AAATTAGCGTAGACATCATTCTCGCTTTGGAAAGCAAGGGTAGTT GGCCCATTTCTACCAAAGAAGGACTTCCCATTCAGGGTTGGCTCG GTACCAAAGTACGCACCAATCTCCGAAGGGAACCTTTCTACCTGG TTCCTAAAAATGCTAAAGATGGAAACTCTTTCCAGGGCGAGACTT GGCGCCTCTCCTTTTCCCACACAGAGAAGTACATCCTTAACAACC ACGGAATCGAAAAAACCTGCTGCGAAAGTTCCGGTGCCAAGTGT TGTCGAAAGGAATGCCTTAAACTGATGAAATACCTTTTGGAGCA GCTCAAAAAGGAATTCCAAGAGCTCGACGCTTTTTGCTCTTACCA CGTTAAGACCGCTATTTTCCACATGTGGACACAGGACCCACAAGA TTCTCAATGGGACCCTAGGAATCTCAGCTCATGTTTCGATAAGTT GTTGGCTTTTTTCCTCGAATGTCTGCGCACCGAGAAGTTGGATCA TTACTTCATTCCCAAGTTCAACCTCTTCTCACAGGAACTGATAGAT CGAAAGTCTAAGGAATTCTTGTCTAAAAAAATAGAGTATGAGCG AAACAATGGTTTCCCCATTTTTGACAAGTTGTGAGCGGCCGCGCG GATCCAGACATGATAA	This paper	Ikegami lab ID: EA087
DNA oligonucleotide EA096 for *Cxcl10* qPCR primer: GCCGTCATTTTCTGCCTCA	This paper	Ikegami lab ID: EA096
DNA oligonucleotide EA097 for *Cxcl10* qPCR primer: CGTCCTTGCGAGAGGGATC	This paper	Ikegami lab ID: EA097
DNA oligonucleotide EA098 for *Ifnb1* qPCR primer: CCTGGAGCAGCTGAATGGAA	This paper	Ikegami lab ID: EA098
DNA oligonucleotide EA099 for *Ifnb1* qPCR primer: TGGATGGCAAAGGCAGTGTAA	This paper	Ikegami lab ID: EA099
DNA oligonucleotide EA100 for *Ifit3* qPCR primer: CCTACATAAAGCACCTAGATGGC	This paper	Ikegami lab ID: EA100
DNA oligonucleotide EA101 for *Ifit3* qPCR primer: ATGTGATAGTAGATCCAGGCGT	This paper	Ikegami lab ID: EA101
DNA oligonucleotide KI444 for *Actb* qPCR primer: CTTTGCAGCTCCTTCGTTGC	This paper	Ikegami lab ID: KI444
DNA oligonucleotide KI445 for *Actb* qPCR primer: CCTTCTGACCCATTCCCACC	This paper	Ikegami lab ID: KI445

DNA oligonucleotide KI466 for AAV titering primer: GCGGATCCAGACATGATAAG	This paper	Ikegami lab ID: KI466
DNA oligonucleotide KI467 for AAV titering primer: GCCTATAGTGAGTCGTATTAAG	This paper	Ikegami lab ID: KI467
Recombinant DNA		
pAAV:cTNT::Luciferase	Addgene	Addgene plasmid #69915
pAAV:cTNT::GFP-GS linker	This paper	Ikegami lab ID: bAE263_1
pAAV:cTNT::GFP-icGAS	This paper	Ikegami lab ID: bAE299_1
pAAV:cTNT::cGAS	This paper	Ikegami lab ID: bAE299_3
pLJM1-EGFP	Addgene	Addgene plasmid #19319
Software and algorithms		
ImageJ	N/A	https://imagej.net/ij/
NIS Elements	Nikon Instruments Inc.	RRID:SCR_014329
Odyssey CLx Imaging System	LI-COR Biosciences	https://www.licor.com/bio/odyssey-dlx/
CellProfiler	Broad Institute	https://cellprofiler.org/
Other		
Bio-Rad CFX96 Real-Time PCR Detection System	Bio-Rad	RRID:SCR_018064
Yokogawa CSU-W1 Sora spinning disk confocal microscope	Nikon Instruments Inc.	https://www.microscope.healthcare.nikon.com/products/confocal-microscopes/csu-series/csu-w1
Nikon A1R laser-scanning confocal microscope	Nikon Instruments Inc.	RRID:SCR_020317

FIGURE 1

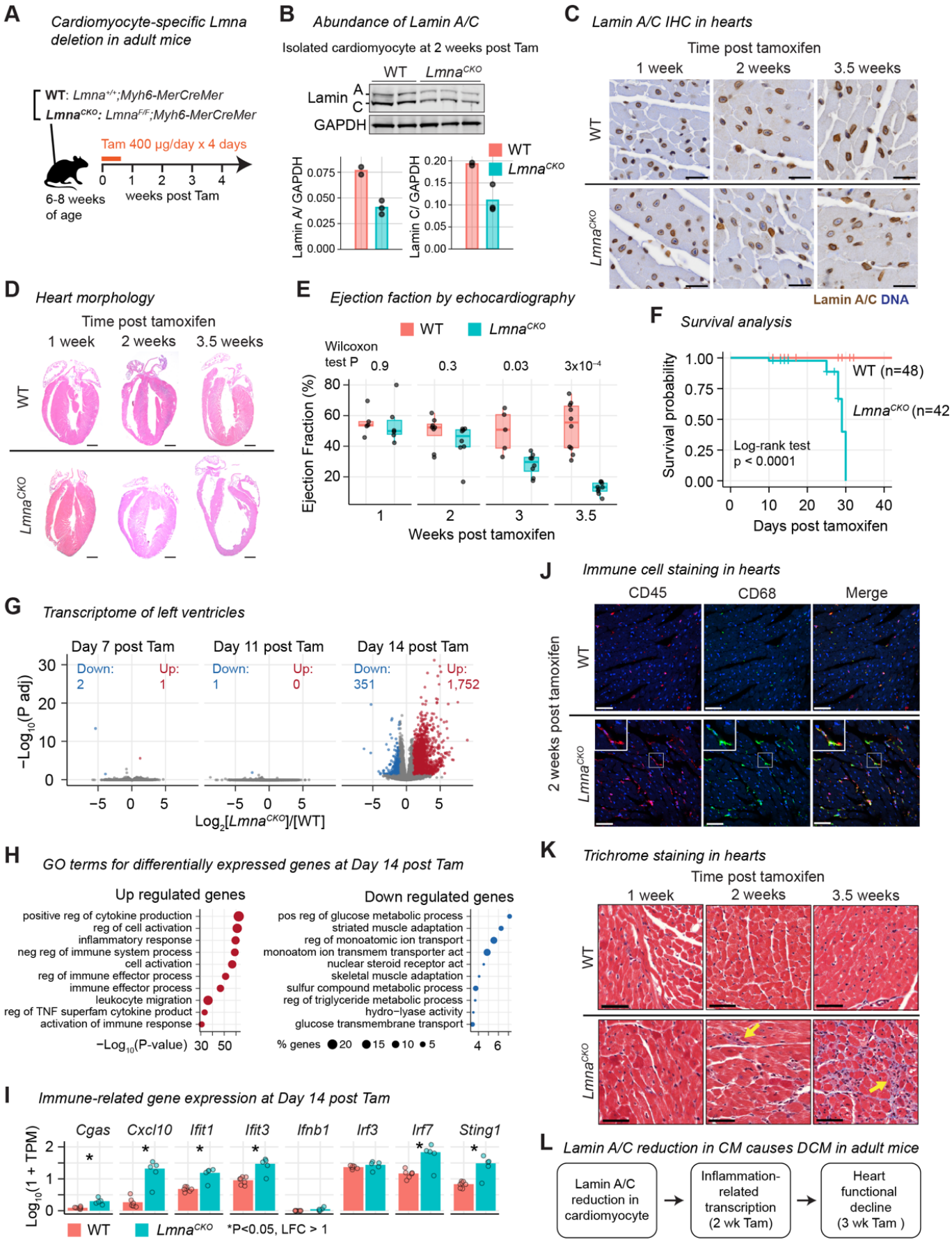
A
Cardiomyocyte-specific Lmna deletion in adult mice
WT: Lmna+/+;Myh6-MerCreMer
LmnaCKO: LmnaF/F;Myh6-MerCreMer
Tam 400 µg/day x 4 days
0 1 2 3 4
weeks post Tam
6-8 weeks of age
B
Abundance of Lamin A/C
Isolated cardiomyocyte at 2 weeks post Tam
WT LmnaCKO
Lamin A C
GAPDH
Lamin A/ GAPDH
Lamin C/ GAPDH
WT
LmnaCKO
C
Lamin A/C IHC in hearts
Time post tamoxifen
1 week 2 weeks 3.5 weeks
WT
LmnaCKO
Lamin A/C DNA
D
Heart morphology
Time post tamoxifen
1 week 2 weeks 3.5 weeks
WT
LmnaCKO
E
Ejection faction by echocardiography
WT LmnaCKO
Wilcoxon test P
0.9 0.3 0.03 3x10−4
Ejection Fraction (%)
Weeks post tamoxifen
F
Survival analysis
Survival probability
WT (n=48)
LmnaCKO (n=42
Log-rank test
p < 0.0001
Days post tamoxifen
G
Transcriptome of left ventricles
Day 7 post Tam
Day 11 post Tam
Day 14 post Tam
Down: 2
Up: 1
Down: 1
Up: 0
Down: 351
Up: 1,752
−Log10(P adj)
Log2[LmnaCKO]/[WT]
H
GO terms for differentially expressed genes at Day 14 post Tam
Up regulated genes
positive reg of cytokine production
reg of cell activation
inflammatory response
neg reg of immune system process
cell activation
reg of immune effector process
immune effector process
leukocyte migration
reg of TNF superfam cytokine product
activation of immune response
−Log10(P-value)
Down regulated genes
pos reg of glucose metabolic process
striated muscle adaptation
reg of monoatomic ion transport
monoatom ion transmem transporter act
nuclear steroid receptor act
skeletal muscle adaptation
sulfur compound metabolic process
reg of triglyceride metabolic process
hydro−lyase activity
glucose transmembrane transport
% genes 20 15 10 5
I
Immune-related gene expression at Day 14 post Tam
Cgas Cxcl10 Ifit1 Ifit3 Ifnb1 Irf3 Irf7 Sting1
Log10(1 + TPM)
WT LmnaCKO
*P<0.05, LFC > 1
J
Immune cell staining in hearts
CD45 CD68 Merge
2 weeks post tamoxifen
WT
LmnaCKO
K
Trichrome staining in hearts
Time post tamoxifen
1 week 2 weeks 3.5 weeks
WT
LmnaCKO
L
Lamin A/C reduction in CM causes DCM in adult mice
Lamin A/C reduction in cardiomyocyte
Inflammation-related transcription (2 wk Tam)
Heart functional decline (3 wk Tam)

FIGURE 2

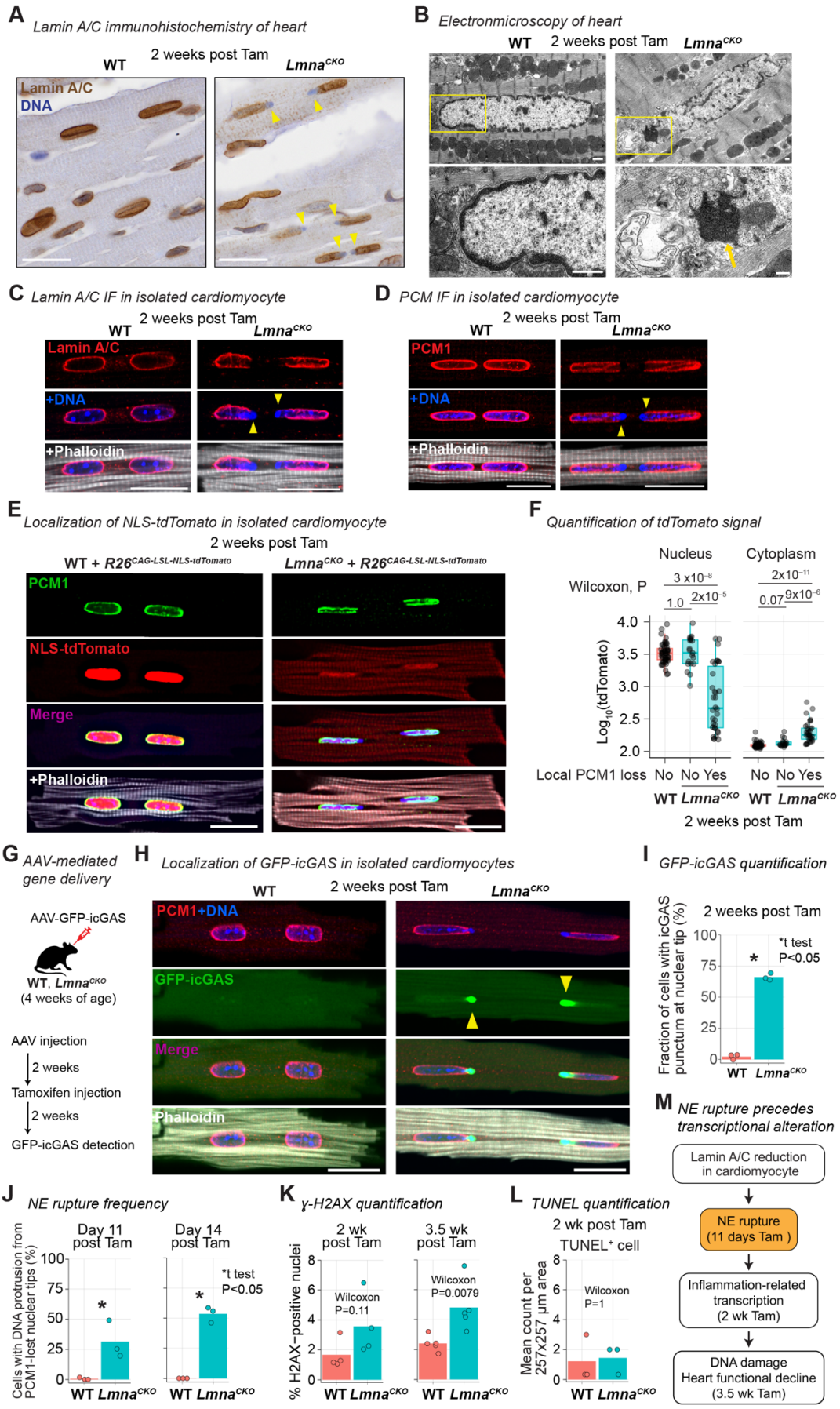
A Lamin A/C immunohistochemistry of heart
WT
2 weeks post Tam
Lmna^CKO
Lamin A/C
DNA
B Electronmicroscopy of heart
WT
2 weeks post Tam
Lmna^CKO
C Lamin A/C IF in isolated cardiomyocyte
2 weeks post Tam
WT
Lmna^CKO
Lamin A/C
+DNA
+Phalloidin
D PCM IF in isolated cardiomyocyte
2 weeks post Tam
WT
Lmna^CKO
PCM1
+DNA
+Phalloidin
E Localization of NLS-tdTomato in isolated cardiomyocyte
2 weeks post Tam
WT + R26^CAG-LSL-NLS-tdTomato
Lmna^CKO + R26^CAG-LSL-NLS-tdTomato
PCM1
NLS-tdTomato
Merge
+Phalloidin
F Quantification of tdTomato signal
Nucleus
Cytoplasm
Wilcoxon, P
3 x10^-8
2x10^-5
1.0
2x10^-11
9x10^-6
0.07
Log10(tdTomato)
4.0
3.5
3.0
2.5
2.0
Local PCM1 loss
No
No
Yes
No
No
Yes
WT
Lmna^CKO
WT
Lmna^CKO
2 weeks post Tam
G AAV-mediated gene delivery
AAV-GFP-icGAS
WT, Lmna^CKO
(4 weeks of age)
AAV injection
2 weeks
Tamoxifen injection
2 weeks
GFP-icGAS detection
H Localization of GFP-icGAS in isolated cardiomyocytes
WT
2 weeks post Tam
Lmna^CKO
PCM1+DNA
GFP-icGAS
Merge
Phalloidin
I GFP-icGAS quantification
2 weeks post Tam
Fraction of cells with icGAS punctum at nuclear tip (%)
100
75
50
25
0
*t test
P<0.05
*
WT
Lmna^CKO
M NE rupture precedes transcriptional alteration
Lamin A/C reduction in cardiomyocyte
NE rupture (11 days Tam)
Inflammation-related transcription (2 wk Tam)
DNA damage
Heart functional decline
(3.5 wk Tam)
J NE rupture frequency
Day 11 post Tam
Day 14 post Tam
Cells with DNA protrusion from PCM1-lost nuclear tips (%)
100
75
50
25
0
*t test
P<0.05
*
*
WT
Lmna^CKO
WT
Lmna^CKO
K γ-H2AX quantification
2 wk post Tam
3.5 wk post Tam
% H2AX−positive nuclei
8
6
4
2
0
Wilcoxon
P=0.11
Wilcoxon
P=0.0079
WT
Lmna^CKO
WT
Lmna^CKO
L TUNEL quantification
2 wk post Tam
TUNEL+ cell
Mean count per 257x257 µm area
8
6
4
2
0
Wilcoxon
P=1
WT
Lmna^CKO

FIGURE 3

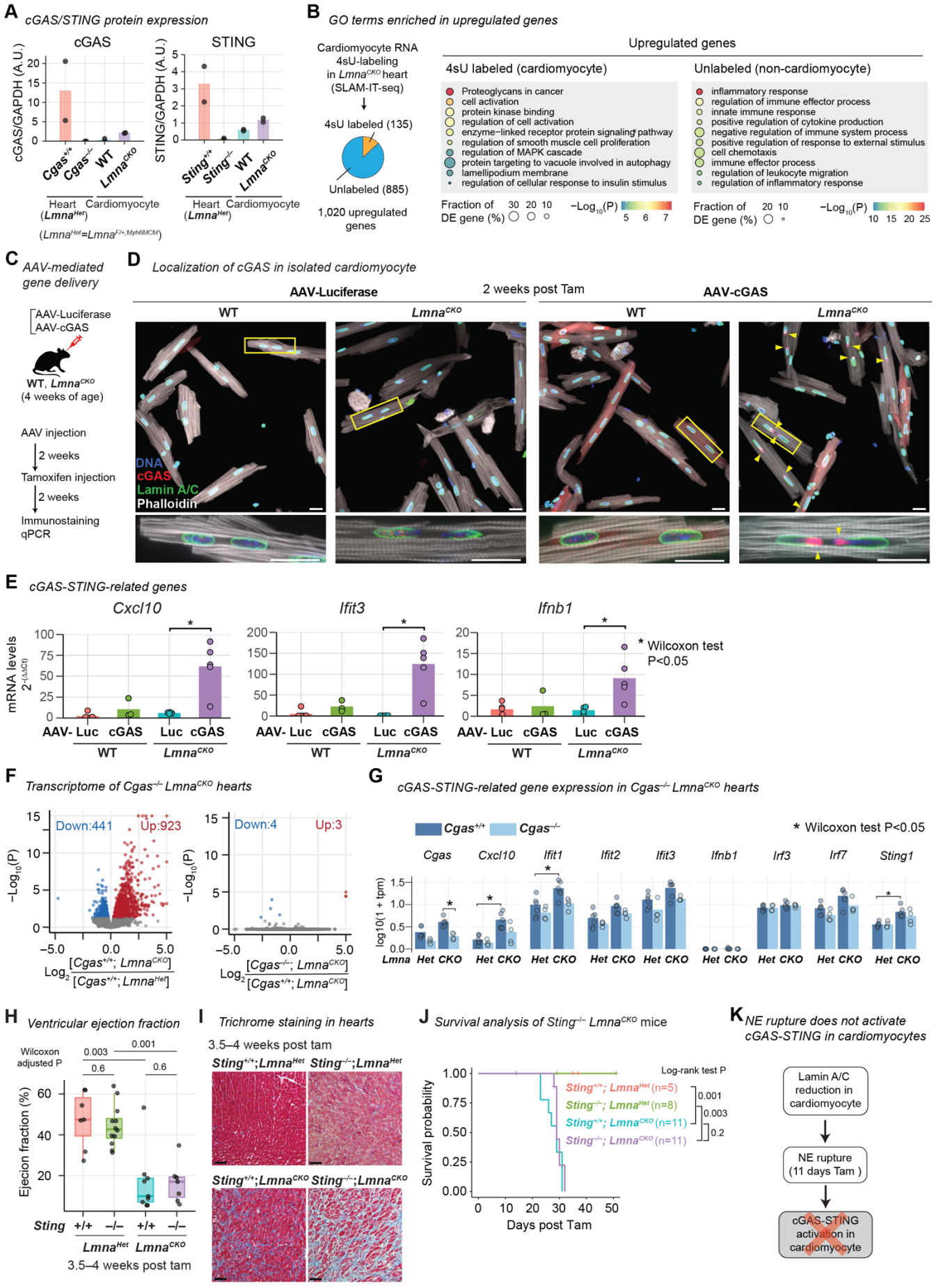
A cGAS/STING protein expression
cGAS
STING
cGAS/GAPDH (A.U.)
STING/GAPDH (A.U.)
Cgas+/+
Cgas−/−
WT
LmnaCKO
Sting+/+
Sting−/−
Heart
Cardiomyocyte
(LmnaHet)
(LmnaHet=LmnaF/+;Myh6MCM)
B GO terms enriched in upregulated genes
Cardiomyocyte RNA 4sU-labeling in LmnaCKO heart (SLAM-IT-seq)
4sU labeled (135)
Unlabeled (885)
1,020 upregulated genes
Upregulated genes
4sU labeled (cardiomyocyte)
Proteoglycans in cancer
cell activation
protein kinase binding
regulation of cell activation
enzyme−linked receptor protein signaling pathway
regulation of smooth muscle cell proliferation
regulation of MAPK cascade
protein targeting to vacuole involved in autophagy
lamellipodium membrane
regulation of cellular response to insulin stimulus
Unlabeled (non-cardiomyocyte)
inflammatory response
regulation of immune effector process
innate immune response
positive regulation of cytokine production
negative regulation of immune system process
positive regulation of response to external stimulus
cell chemotaxis
immune effector process
regulation of leukocyte migration
regulation of inflammatory response
Fraction of DE gene (%)
−Log10(P)
C AAV-mediated gene delivery
AAV-Luciferase
AAV-cGAS
WT, LmnaCKO
(4 weeks of age)
AAV injection
2 weeks
Tamoxifen injection
2 weeks
Immunostaining
qPCR
D Localization of cGAS in isolated cardiomyocyte
AAV-Luciferase
2 weeks post Tam
AAV-cGAS
WT
LmnaCKO
DNA
cGAS
Lamin A/C
Phalloidin
E cGAS-STING-related genes
Cxcl10
Ifit3
Ifnb1
mRNA levels
2−(ΔΔCt)
AAV-
Luc
cGAS
* Wilcoxon test P<0.05
F Transcriptome of Cgas−/− LmnaCKO hearts
Down:441
Up:923
Down:4
Up:3
−Log10(P)
Log2 [Cgas+/+; LmnaCKO] / [Cgas+/+; LmnaHet]
Log2 [Cgas−/−; LmnaCKO] / [Cgas+/+; LmnaCKO]
G cGAS-STING-related gene expression in Cgas−/− LmnaCKO hearts
Cgas+/+
Cgas−/−
* Wilcoxon test P<0.05
Cgas
Cxcl10
Ifit1
Ifit2
Ifit3
Ifnb1
Irf3
Irf7
Sting1
log10(1 + tpm)
Lma
Het
CKO
H Ventricular ejection fraction
Wilcoxon adjusted P
0.003
0.001
0.6
0.6
Ejecion fraction (%)
Sting
+/+
−/−
LmnaHet
LmnaCKO
3.5–4 weeks post tam
I Trichrome staining in hearts
3.5–4 weeks post tam
Sting+/+;LmnaHet
Sting−/−;LmnaHet
Sting+/+;LmnaCKO
Sting−/−;LmnaCKO
J Survival analysis of Sting−/− LmnaCKO mice
Log-rank test P
Sting+/+; LmnaHet (n=5)
Sting−/−; LmnaHet (n=8)
Sting+/+; LmnaCKO (n=11)
Sting−/−; LmnaCKO (n=11)
0.001
0.003
0.2
Survival probability
Days post Tam
K NE rupture does not activate cGAS-STING in cardiomyocytes
Lamin A/C reduction in cardiomyocyte
NE rupture (11 days Tam)
cGAS-STING activation in cardiomyocyte

FIGURE 4

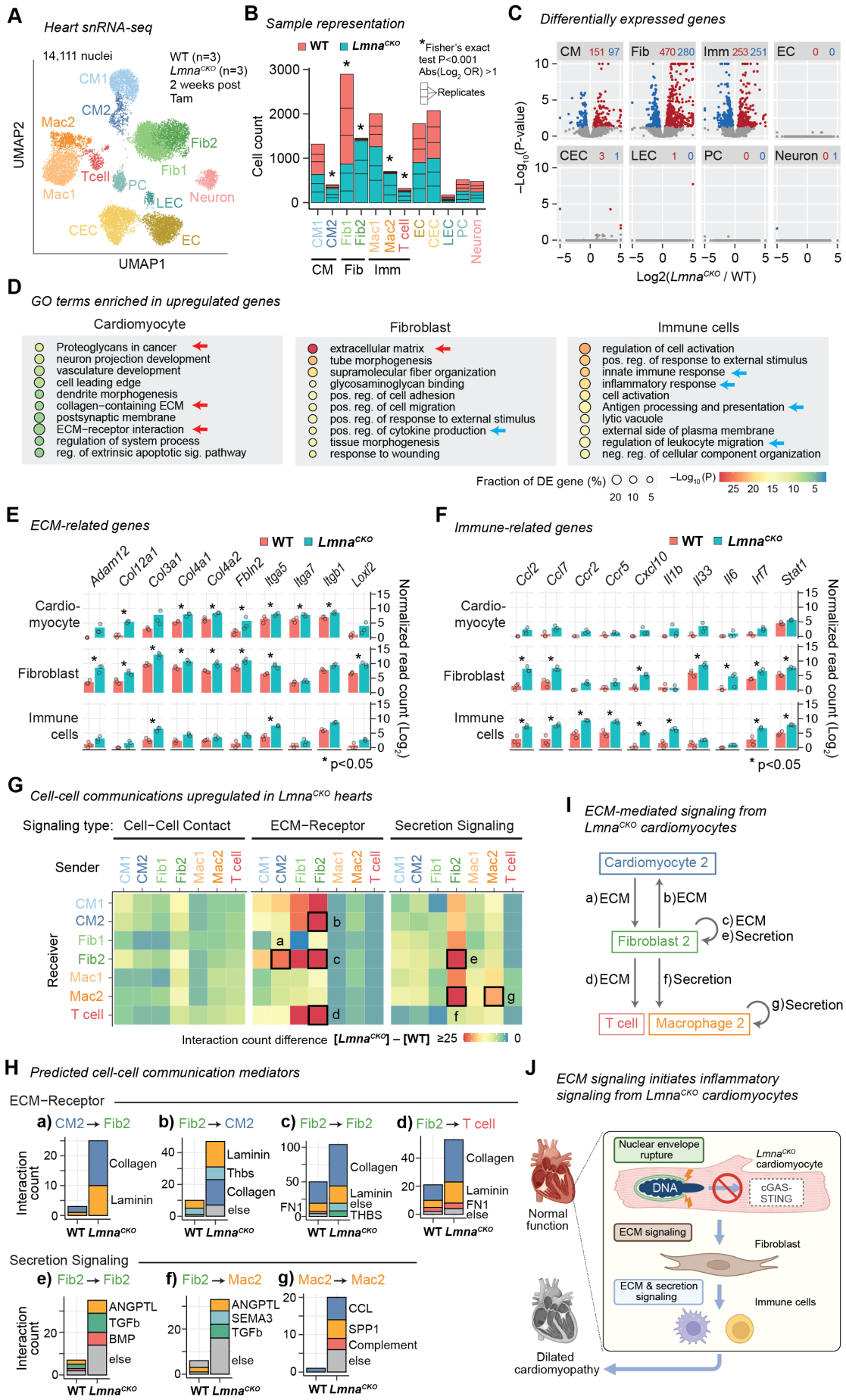
A
Heart snRNA-seq
14,111 nuclei
WT (n=3)
Lmna^CKO (n=3)
2 weeks post Tam
CM1
CM2
Mac2
Fib2
Fib1
Tcell
PC
Mac1
LEC
Neuron
CEC
EC
UMAP2
UMAP1
B
Sample representation
WT
Lmna^CKO
*Fisher's exact test P<0.001 Abs(Log2 OR) >1
Replicates
Cell count
CM
Fib
Imm
C
Differentially expressed genes
CM 151 97
Fib 470 280
Imm 253 251
EC 0 0
CEC 3 1
LEC 1 0
PC 0 0
Neuron 0 1
−Log10(P-value)
Log2(Lmna^CKO / WT)
D
GO terms enriched in upregulated genes
Cardiomyocyte
Proteoglycans in cancer
neuron projection development
vasculature development
cell leading edge
dendrite morphogenesis
collagen−containing ECM
postsynaptic membrane
ECM−receptor interaction
regulation of system process
reg. of extrinsic apoptotic sig. pathway
Fibroblast
extracellular matrix
tube morphogenesis
supramolecular fiber organization
glycosaminoglycan binding
pos. reg. of cell adhesion
pos. reg. of cell migration
pos. reg. of response to external stimulus
pos. reg. of cytokine production
tissue morphogenesis
response to wounding
Immune cells
regulation of cell activation
pos. reg. of response to external stimulus
innate immune response
inflammatory response
cell activation
Antigen processing and presentation
lytic vacuole
external side of plasma membrane
regulation of leukocyte migration
neg. reg. of cellular component organization
Fraction of DE gene (%)
−Log10(P)
E
ECM-related genes
Adam12
Col12a1
Col3a1
Col4a1
Col4a2
Fbln2
Itga5
Itga7
Itgb1
Loxl2
Cardio-myocyte
Fibroblast
Immune cells
Normalized read count (Log2)
* p<0.05
F
Immune-related genes
Ccl2
Ccl7
Ccr2
Ccr5
Cxcl10
Il1b
Il33
Il6
Irf7
Stat1
G
Cell-cell communications upregulated in Lmna^CKO hearts
Signaling type: Cell−Cell Contact
ECM−Receptor
Secretion Signaling
Sender
Receiver
Interaction count difference [Lmna^CKO] − [WT] ≥25
I
ECM-mediated signaling from Lmna^CKO cardiomyocytes
Cardiomyocyte 2
a) ECM
b) ECM
c) ECM
e) Secretion
Fibroblast 2
d) ECM
f) Secretion
g) Secretion
T cell
Macrophage 2
H
Predicted cell-cell communication mediators
ECM−Receptor
a) CM2 → Fib2
b) Fib2 → CM2
c) Fib2 → Fib2
d) Fib2 → T cell
Interaction count
Collagen
Laminin
Thbs
else
FN1
THBS
Secretion Signaling
e) Fib2 → Fib2
f) Fib2 → Mac2
g) Mac2 → Mac2
ANGPTL
TGFb
BMP
SEMA3
CCL
SPP1
Complement
WT Lmna^CKO
J
ECM signaling initiates inflammatory signaling from Lmna^CKO cardiomyocytes
Normal function
Dilated cardiomyopathy
Nuclear envelope rupture
Lmna^CKO cardiomyocyte
DNA
cGAS-STING
ECM signaling
Fibroblast
ECM & secretion signaling
Immune cells

SUPPLEMENTARY FIGURE S1

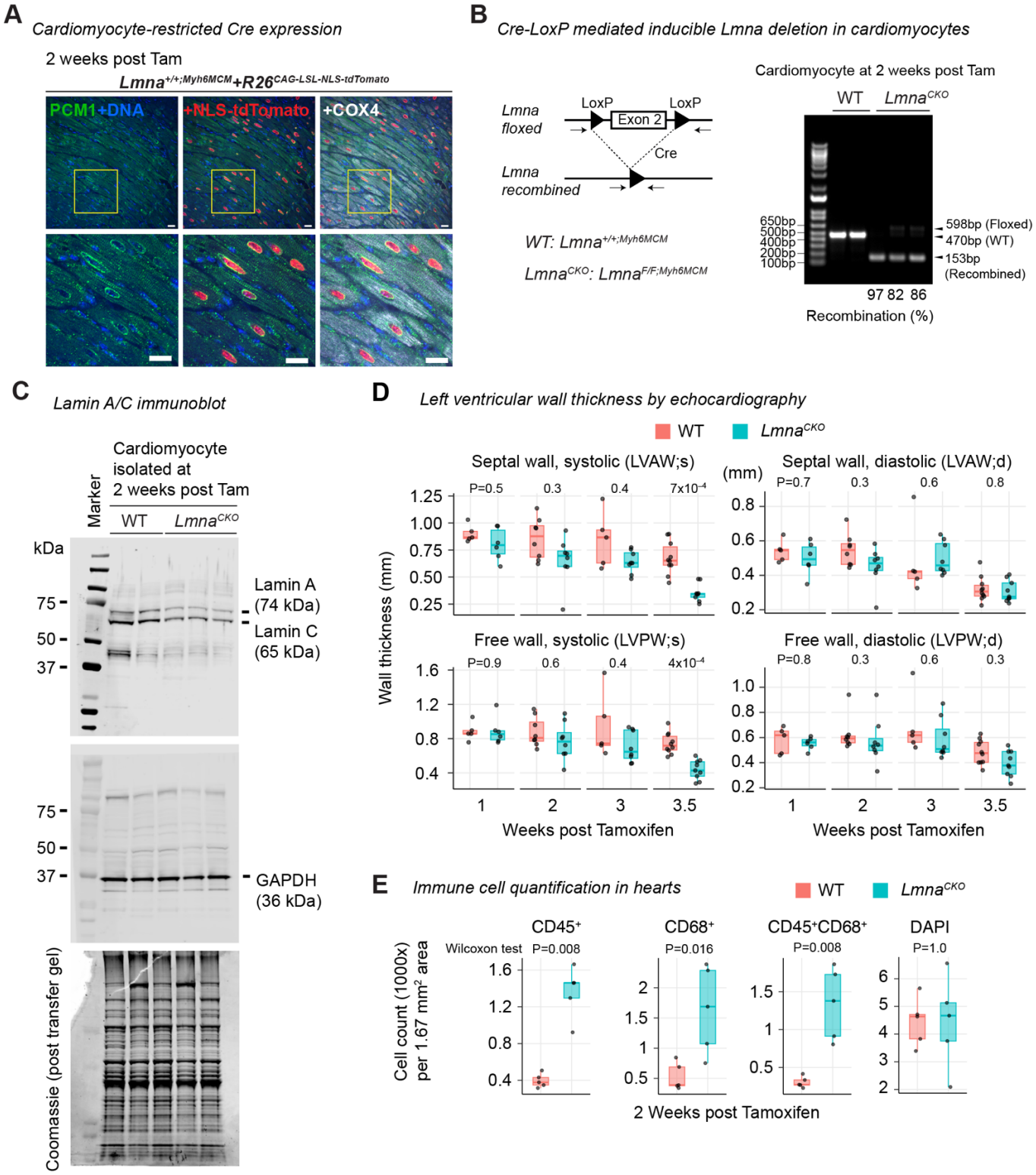

1128

SUPPLEMENTARY FIGURE S2

A *Additional images for EM in hearts*

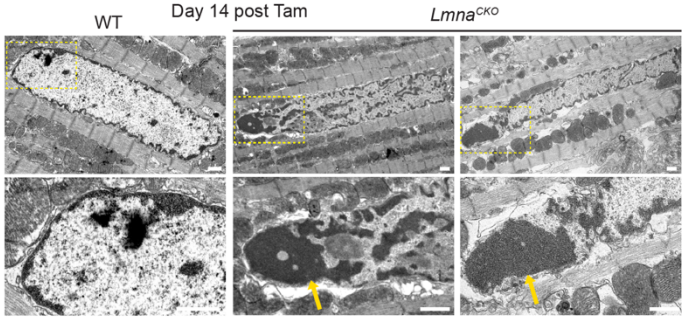

B *Additional images for NLS-tdTomato signals in Lmna^CKO CMs*

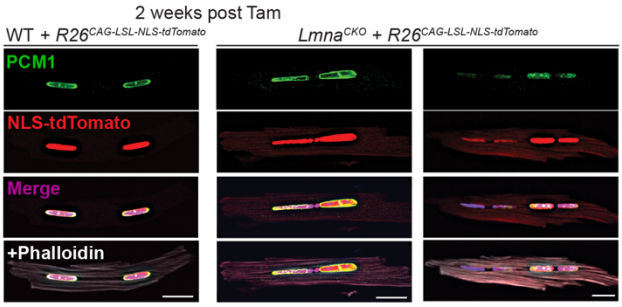

C *Localization of cytoplasmic DNA sensor GFP-icGAS in isolated cardiomyocytes*

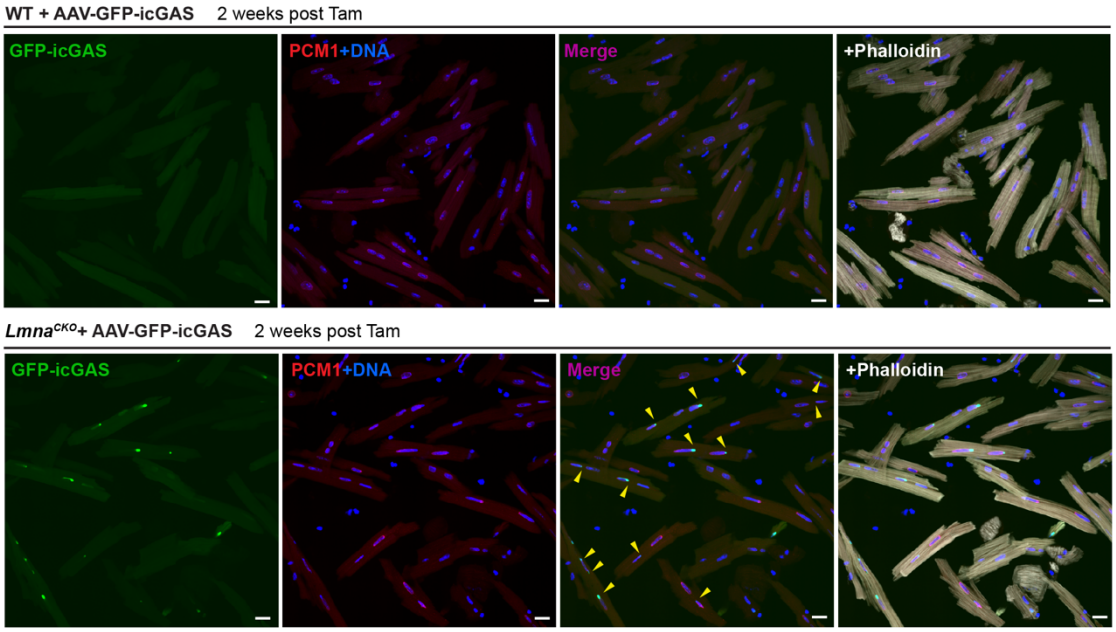

D *PCM1 IF in CMs at Day 11 post Tam*

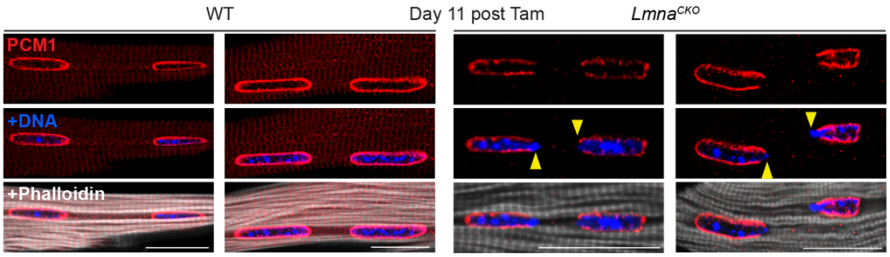

E *Number of nuclei with DNA protrusion from PCM1-lost nuclear tips per cell*

		No. nuclei with DNA protrusion from PCM1-lost nuclear tips		
		0	1	≥2
% Cells (count)				
Day 11 post Tam	WT	99% (163)	1% (1)	0% (0)
	Lmna^CKO	69% (121)	14% (25)	17% (30)
Day 14 post Tam	WT	100% (163)	0% (0)	0% (0)
	Lmna^CKO	46% (78)	25% (42)	29% (49)

F *γ-H2AX IF in heart*

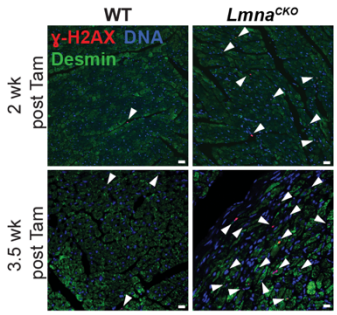

G *TUNEL assay in heart section*

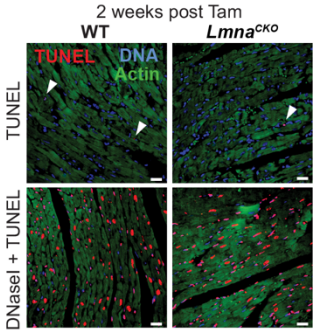

SUPPLEMENTARY FIGURE S3

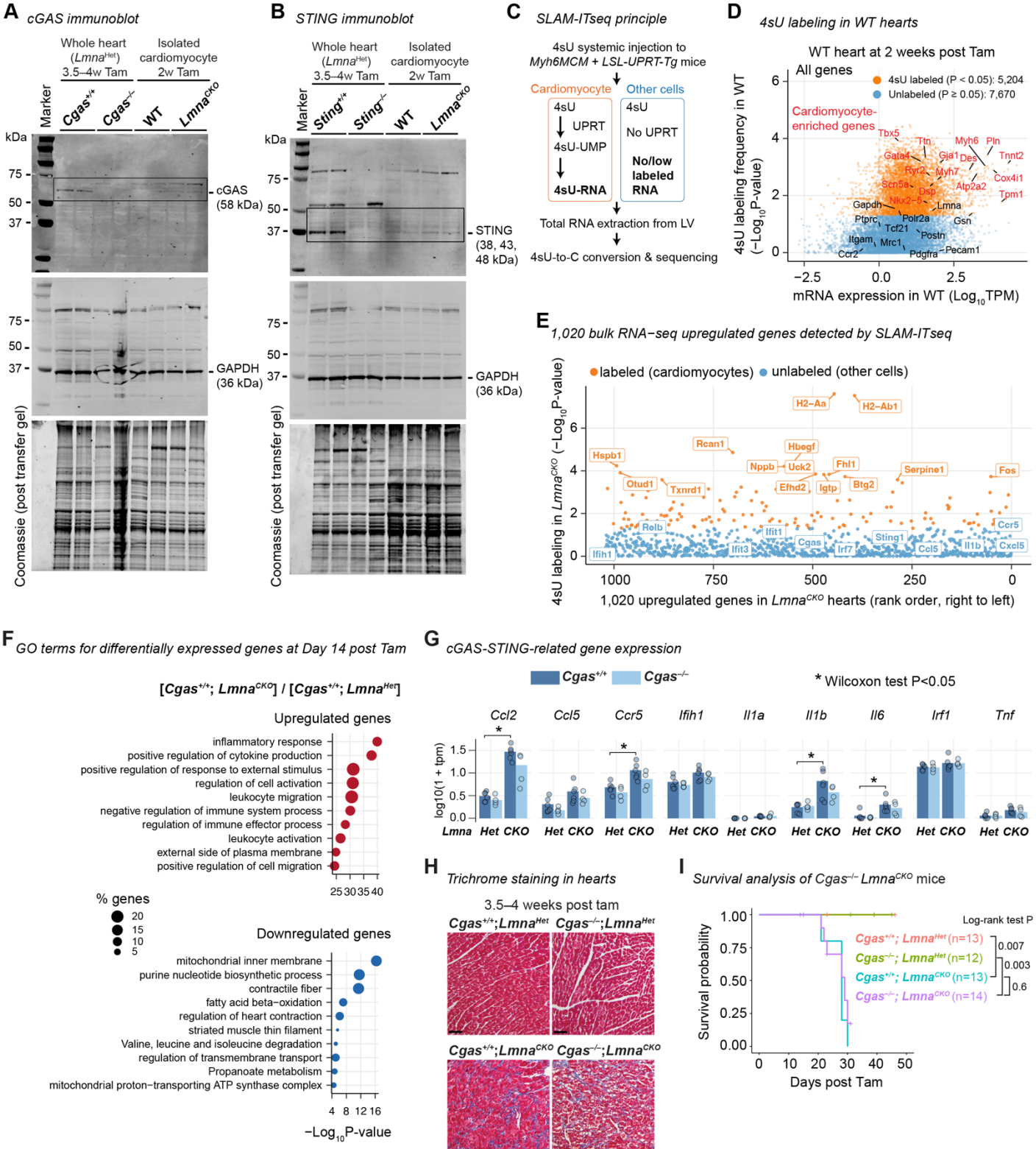

1131

SUPPLEMENTARY FIGURE S4

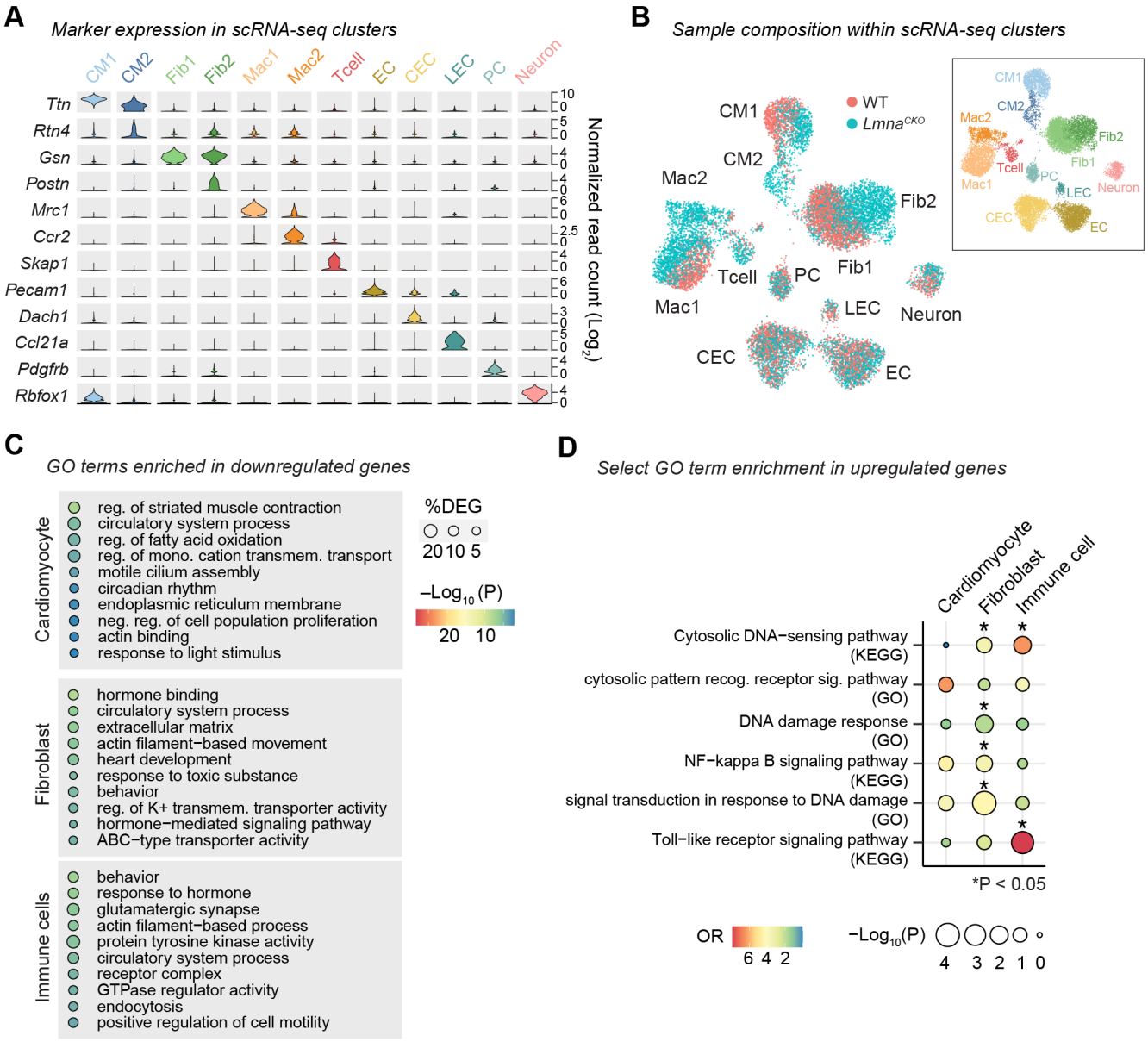

1132